Dynamic Hybrid Beamforming With Low-Resolution PSs for Wideband mmWave MIMO-OFDM Systems

Hongyu Li, *Graduate Student Member, IEEE*, Ming Li, *Senior Member, IEEE*, Qian Liu, *Member, IEEE*, and A. Lee Swindlehurst, *Fellow, IEEE*

***Abstract*— Analog/digital hybrid beamforming is considered as a key enabling multiple antenna technology for implementing millimeter wave (mmWave) multiple-input multiple-output (MIMO) communications since it can reduce the number of costly and power-hungry radio frequency (RF) chains while still providing for spatial multiplexing. In this paper, we introduce a novel hybrid beamforming architecture with dynamic antenna subarrays and hardware-efficient low-resolution phase shifters (PSs) for a wideband mmWave MIMO orthogonal frequency division multiplexing (MIMO-OFDM) system. By dynamically connecting each RF chain to a non-overlapping antenna subarray via a switch network and PSs, multiple-antenna diversity can be exploited to mitigate the performance loss due to the employment of practical low-resolution PSs. For this dynamic hybrid beamforming architecture, we jointly design the hybrid precoder and combiner to maximize the average spectral efficiency of the mmWave MIMO-OFDM system. In particular, the spectral efficiency maximization problem is first converted to a mean square error (MSE) minimization problem. Then, an efficient iterative hybrid beamformer algorithm is developed based on classical block coordination descent (BCD) methods. An analysis of the convergence and complexity of the proposed algorithm is also provided. Extensive simulation results demonstrate the superiority of the proposed hybrid beamforming algorithm with dynamic subarrays and low-resolution PSs.**

***Index Terms*— Millimeter wave (mmWave) communications, multiple-input multiple-output (MIMO), hybrid beamforming, dynamic antenna subarrays, low-resolution phase shifters (PSs).**

I. Introduction

THE fast development of emerging applications (e.g. virtual reality, holographic imaging, artificial intelligence, etc.) and exponential growth in the volume of wireless data have motivated the use of the large amount of underutilized spectrum in millimeter wave (mmWave) bands in fifth-generation (5G) and beyond networks [1], [2]. The shorter wavelength of mmWave signals combined with massive multiple-input multiple-output (MIMO) architectures can provide sufficient beamforming gains to combat the severe path loss in mmWave channels and achieve highly directional beamforming to finely control interference among users/cells [3].

For mmWave massive MIMO systems, conventional fully-digital beamforming architectures require one dedicated radio-frequency (RF) chain (including analog-to-digital/digital-to-analog converter (ADC/DAC), etc.) for each antenna. However, fully-digital beamforming is not viable due to the high cost and power consumption of large numbers of mmWave RF chains and other hardware components, especially at high frequencies [4], [5]. In order to overcome the challenge of the hardware limitations while still providing for the multiplexing/multi-user transmissions, analog/digital hybrid beamforming has been advocated as a promising solution for mmWave massive MIMO systems [6]–[8]. In particular, the hybrid beamforming architecture divides the spatial signal processing into a combination of high-dimentional analog beamforming realized by a large number of cost-efficient phase shifters (PSs) to compensate for the severe path loss of mmWave channel together with low-dimensional digital beamforming to realize the multiplexing/multi-user transmissions.

A. Prior Work

In the last few years, hybrid beamforming has received considerable interest in both academia and industry. Extensive work has been carried out to investigate different hybrid beamforming architectures and/or beamformer designs for mmWave MIMO systems. Fully-connected architectures, in which each RF chain is connected to all antennas via a PS network, is one of the most popular hybrid beamforming implementations due to its superiority in achieving performance close to that of fully-digital solutions. Considering this fully-connected architecture, in [9], [10] hybrid beamformer designs were developed to minimize the Euclidean distance between the hybrid beamformer and the optimal fully-digital beamformer. Codebook-based hybrid beamforming is an alternative widely-used solution [11]–[13], in which

Manuscript received October 1, 2019; revised January 15, 2020; accepted February 17, 2020. Date of publication June 8, 2020; date of current version August 28, 2020. This work was supported in part by the National Natural Science Foundation of China under Grant 61971088, Grant 61671101, and Grant 61761136019, in part by the Natural Science Foundation of Liaoning Province under Grant 20180520019, and in part by the U.S. National Science Foundation under Grant CCF-1703635 and Grant ECCS-1824565. *(Corresponding author: Ming Li.)*

Hongyu Li and Ming Li are with the School of Information and Communication Engineering, Dalian University of Technology, Dalian 116024, China (e-mail: hongyuli@mail.dlut.edu.cn; mli@dlut.edu.cn).

Qian Liu is with the School of Computer Science and Technology, Dalian University of Technology, Dalian 116024, China (e-mail: qianliu@dlut.edu.cn).

A. Lee Swindlehurst is with the Center for Pervasive Communications and Computing, University of California at Irvine, Irvine, CA 92697 USA (e-mail: swindle@uci.edu).

Color versions of one or more of the figures in this article are available online at http://ieeexplore.ieee.org.

Digital Object Identifier 10.1109/JSAC.2020.3000878

the analog beamformers are selected from pre-arranged candidate vectors (e.g. beam steering vectors and discrete Fourier transform (DFT) beamformers). Other approaches [14]–[16] design the hybrid beamformer based on the minimum mean square error (MMSE) criterion.

Although fully-connected hybrid beamforming is very hardware efficient compared with fully-digital beamforming, the use of large numbers of PSs may still cause relatively high hardware complexity and power consumption. Thus, extensions to partially-connected architectures have also been studied [17]–[19]. In the partially-connected architecture, each RF chain is connected to a fixed non-overlapping subset of the antennas and forms an analog beamformer for this antenna subarray. Therefore, the number of PSs can be greatly reduced and the energy-and-hardware efficiency can be improved with little sacrifice in spectral efficiency.

Nevertheless, the previous work in [9]–[19] generally assumed the use of *infinite/high-resolution* PSs, which still has high hardware complexity at mmWave frequencies [4]. In realistic mmWave systems, low resolution but less expensive PSs are more practical for realizing analog beamformers. Therefore, in addition to reducing the number of PSs by partially-connected architectures, utilizing *low-resolution* PSs is another approach to reduce the cost and the power consumption [20]. Hybrid beamforming with low-resolution PSs has been investigated for fully-connected architectures in [21]–[23]. While employing low-resolution PSs for partially-connected hybrid beamforming can achieve maximum hardware-and-energy efficiency, traditional fixed subarray hybrid beamforming schemes cannot always provide satisfactory spectral efficiency [24], [25] for the following two reasons: *i*) The employment of low-resolution PSs makes it difficult to finely control the beam and thus will reduce beamforming accuracy; *ii)* the fixed-subarray architecture limits the flexibility of large antenna arrays and further causes notable performance degradation.

Recently, dynamic subarray strategies, which adaptively partition all transmit/receive antennas into several subarrays and connects/maps each RF chain to one of them, have been proposed to provide more flexibility than fixed subarrays. Several papers have demonstrated the benefits on both spectral efficiency and energy efficiency of applying a dynamic connection strategy for hybrid beamforming with infinite/finite resolution PSs [26]–[31]. Moreover, recent work [32], [33] has illustrated that dynamic antenna selection can effectively compensate for the accuracy loss of the low-resolution PSs. Motivated by these findings, in our previous work [34], we proposed a novel hybrid beamforming architecture with dynamic subarrays and low-resolution PSs for mmWave multi-user multi-input single-output (MU-MISO) systems. With the aid of the theory of fractional programming, an iterative hybrid beamformer algorithm was developed to maximize the sum-rate performance of the mmWave MU-MISO system.

The hybrid beamforming approaches using low-resolution PSs mentioned above are restricted to narrowband mmWave MIMO/MISO channels. However, mmWave communication systems are expected to operate with wide bandwidths in order to exploit the abundant available frequency spectrum.

TABLE I
SUMMARY OF EXISTING DYNAMIC HYBRID BEAMFORMING RESEARCH

	Narrowband	Wideband
Continuous phase	[29], [30]	[26]-[28]
Low resolution	[31], [34]	This work

The frequency selectivity of wideband channels and the unique structure of hybrid beamforming cause difficulties for mmWave wideband MIMO systems. The main challenge lies in designing a common analog beamformer shared for all frequencies/subcarriers while using different digital beamformers for different sub-bands. This motivates the investigation of hybrid beamforming designs for wideband mmWave MIMO-OFDM systems [26]–[28], [35]–[37]. In particular, [26]–[28] investigated partially-connected hybrid precoder design with dynamic subarrays for MIMO-OFDM systems, but using infinite-resolution PSs. To the best of our knowledge, *dynamic* hybrid beamforming with *low-resolution* PSs for *wideband* mmWave MIMO-OFDM systems has not been studied.

While the frequency selectivity of the wideband channel must be considered, the beam squint effect [38]–[40] should also be accounted for in hybrid beamformer designs for wideband mmWave MIMO-OFDM systems. The beam squint effect in communications systems is firstly pointed out in [38], [39], where the necessity of considering beam squint in wideband mmWave systems is strongly demonstrated. Specifically, with a common analog beamformer for all subcarriers, the beam focusing direction will change for different frequencies, an effect referred to as "beam squint". Beam squint introduces array gain variations over subcarriers for a given angle of arrival/departure (AoA/AoD). Obviously, the beam squint effect has a significant impact on the performance of hybrid beamforming in wideband mmWave MIMO-OFDM systems. Relatively little work [41], [42] has taken both frequency selectivity and beam squint into account for fully-connected hybrid beamformer designs. This motivates us to develop an effective dynamic hybrid beamformer algorithm that considers both frequency selectivity and beam squint for wideband mmWave MIMO-OFDM channels.

B. Contributions

The contributions of this paper are summarized as follows:

- We introduce an efficient hybrid beamforming architecture with dynamic subarrays and low-resolution PSs for a wideband mmWave MIMO-OFDM system. In order to mitigate the performance loss due to the use of low-resolution PSs, each RF chain is adaptively connected to a disjoint subset of the transmit/receive antennas to exploit multi-antenna diversity of large-scale antenna arrays.
- We design the hybrid precoder and combiner to maximize the average spectral efficiency of the wideband mmWave MIMO-OFDM system. Compared with existing dynamic hybrid beamforming works as summarized in Table I, this paper considers both *low-resolution* PSs and *wideband* systems, which will cause significant difficulty in the

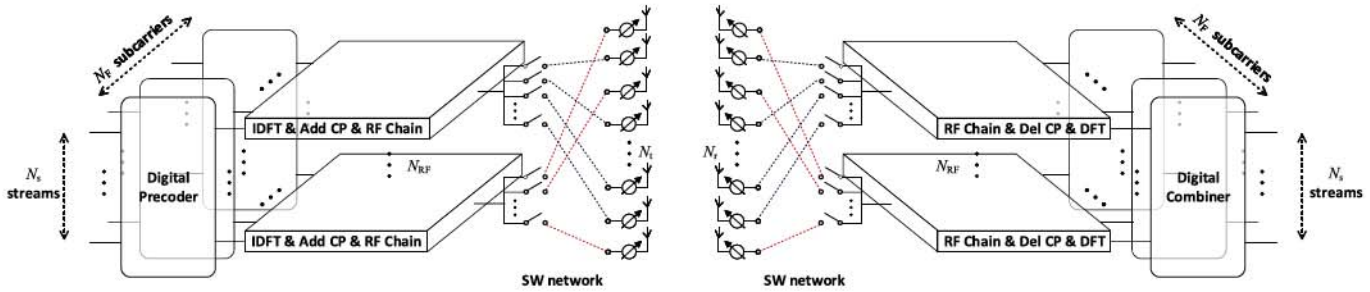

Fig. 1. Dynamic hybrid beamforming with low-resolution PSs for mmWave MIMO-OFDM system.

dynamic hybrid beamformer design. Moreover, while existing works only focus on designing the hybrid precoder for the transmitter side, this work considers joint hybrid precoder and combiner design for both transmitter and receiver sides, which is clearly a more complex problem. With the aid of the equivalence of spectral efficiency maximization and MSE minimization, an effective iterative hybrid beamformer design algorithm is developed using classical block coordination descent (BCD) methods.

- The convergence of the proposed hybrid beamformer algorithm is theoretically proved and numerically illustrated. The time complexity of the proposed hybrid beamformer design is also provided.
- The performance of the proposed hybrid beamformer design is also validated by extensive simulations, which illustrate that the proposed algorithm can significantly outperform traditional fixed-subarray schemes.

The following notations are used throughout this paper. Boldface lower-case letters indicate column vectors and boldface upper-case letters indicate matrices, respectively. $\mathbb{C}$, $\mathbb{R}$, and $\mathbb{R}^+$ denote the set of complex, real, and positive real numbers, respectively. $(\cdot)^*$ denotes the conjugate operation on a complex number. $(\cdot)^T$, $(\cdot)^H$, $(\cdot)^{-1}$ and $(\cdot)^\dagger$ denote the transpose, conjugate-transpose operations, inversion, and pseudo-inversion respectively. $\mathbb{E}\{\cdot\}$ represents statistical expectation. $\Re\{\cdot\}$ denotes the real part of a complex number. $\mathbf{I}_L$ indicates an $L\times L$ identity matrix. $\|\mathbf{A}\|_F$ denotes the Frobenius norm of matrix $\mathbf{A}$. $\|\mathrm{a}\|_0$ is the 0-norm of vector a. Finally, $\mathbf{A}(i,:)$, $\mathbf{A}(:,j)$, and $\mathbf{A}(i,j)$ denote the i-th row, j-th column, and (i,j)-th element of matrix $\mathbf{A}$, respectively. The distribution of a circularly symmetric complex Gaussian (CSCG) random vector variable with mean $\boldsymbol{\mu}$ and covariance matrix $\mathbf{C}$ is denoted by $\mathcal{CN}(\boldsymbol{\mu},\mathbf{C})$, and "$\sim$" stands for "distributed as".

II. System Model and Problem Formulation

A. System Model

We begin by considering a point-to-point mmWave MIMO-OFDM system as shown in Fig. 1. A hybrid beamforming MIMO-OFDM architecture with N_{F} subcarriers is implemented at the transmitter and receiver. The transmitter employs a uniform planar array (UPA) with $N_{\mathrm{t}} = N_{\mathrm{x}}^{\mathrm{t}} \times N_{\mathrm{y}}^{\mathrm{t}}$ antennas and $N_{\mathrm{RF}}^{\mathrm{t}}$ RF chains to simultaneously transmit N_{s} data streams to the receiver which is equipped with $N_{\mathrm{r}} = N_{\mathrm{x}}^{\mathrm{r}} \times N_{\mathrm{y}}^{\mathrm{r}}$ antennas and $N_{\mathrm{RF}}^{\mathrm{r}}$ RF chains. We assume in this paper that the number of RF chains is much less than the number of antennas and greater than or equal to the number of data streams on both sides, i.e. $N_{\mathrm{s}} \le N_{\mathrm{RF}}^{\mathrm{t}} \ll N_{\mathrm{t}}$, $N_{\mathrm{s}} \le N_{\mathrm{RF}}^{\mathrm{r}} \ll N_{\mathrm{r}}$. The main difference between OFDM-based hybrid beamforming and fully-digital beamforming is that the digital beamforming is performed in the frequency domain for each subcarrier while the analog beamforming is performed in the time domain for all subcarriers simultaneously. Next, we describe the components of the system in more detail.

1) Transmitter: Let $\mathrm{s}_i \in \mathbb{C}^{N_{\mathrm{s}}}$ be the symbols to be transmitted via the i-th subcarrier, $\mathbb{E}\{\mathrm{s}_i\mathrm{s}_i^H\} = \mathbf{I}_{N_{\mathrm{s}}}$, $i = 1,\ldots,N_{\mathrm{F}}$. The vector s_i is firstly precoded by a digital beamforming matrix $\mathbf{F}_{\mathrm{BB},i} \in \mathbb{C}^{N_{\mathrm{RF}}^{\mathrm{t}}\times N_{\mathrm{s}}}, i = 1,\ldots,N_{\mathrm{F}}$, in the frequency domain. After conversion to the time domain by the inverse discrete Fourier transform (IDFT) and adding the cyclic prefix, the signals are up-converted to the RF domain via $N_{\mathrm{RF}}^{\mathrm{t}}$ RF chains and further precoded in the analog domain. In order to reduce the hardware complexity and power consumption, N_{t} low-resolution PSs are employed to implement the analog beamformers. In this paper, we adopt a dynamic mapping between RF chains and transmit/receive antennas. Specifically, each RF chain can be dynamically connected to a disjoint set of antennas via a switch (SW) network and corresponding low-resolution PSs. While switches designed for mmWave systems can switch at speeds on the order of nanoseconds or even sub-nanoseconds [43], the coherence time for a carrier frequency $f_{\mathrm{c}} = 60$GHz is about 1ms at a 800Hz Doppler [44]. Therefore, the switching rates and settling times for currently available RF switches are sufficient for the proposed wideband mmWave systems. Since the insertion loss of mmWave switches is extremely low (about 1dB [43]), it can also be ignored in practical mmWave systems. Moreover, the discussion in [6], [26], [50] also illustrated the feasibility of using switches in hybrid beamforming architectures for mmWave massive MIMO systems.

Each low-resolution PS has a constant magnitude $\frac{1}{\sqrt{N_{\mathrm{t}}}}$ and discrete phases controlled by b bits. The set of phase values for each PS is assumed to be uniformly spaced around the unit circle, i.e. $\mathcal{F} = \{\frac{1}{\sqrt{N_{\mathrm{t}}}} e^{j\frac{2\pi i}{2^b}} | i = 0,1,\ldots,2^b-1\}$. By dynamically selecting antennas and tuning the phases of the associated PSs, the size of each subarray and the corresponding analog beamformer are properly selected according to the instantaneous channel state information (CSI). By exploiting the degrees of freedom introduced by the SW network, the flexibility of the dynamic mapping scheme and the multi-antenna diversity can be used to appropriately compensate for the loss in accuracy due to the use of low-resolution PSs. This fact will

be demonstrated in the simulation part (e.g. Figs. 4 and 5). Let $\mathbf{F}_{\mathrm{RF}} \in \{\mathcal{F}, 0\}^{N_{\mathrm{t}} \times N_{\mathrm{RF}}}$ be the analog precoding matrix. To be concrete, the analog precoder has two constraints due to the assumed hardware structure: *i)* If the k-th RF chain is connected to the m-th antenna via a low-resolution PS, then the corresponding element of the analog precoder has a nonzero value, i.e. $\mathbf{F}_{\mathrm{RF}}(m,k) \in \mathcal{F}$; otherwise, $\mathbf{F}_{\mathrm{RF}}(m,k) = 0$; *ii)* Since there is no overlap among subarrays, the analog precoder has only one nonzero elements in each row, i.e. $\|\mathbf{F}_{\mathrm{RF}}(m,:)\|_0 = 1, m = 1, \ldots, N_{\mathrm{t}}$.

2) Receiver: After propagating through the wideband mmWave MIMO channel, the signal is corrupted by additive white Gaussion noise (AGWN). At the receiver, which has an architecture similar to the transmitter, the received signal is first processed by N_{r} low-resolution PSs and SWs which form the analog combiner $\mathbf{W}_{\mathrm{RF}}$. The analog combiner $\mathbf{W}_{\mathrm{RF}}$ has constraints similar to the analog precoder: *i)* Each nonzero element has discrete phase and constant amplitude, i.e. $\mathbf{W}_{\mathrm{RF}} \in \{\mathcal{W}, 0\}^{N_{\mathrm{r}} \times N_{\mathrm{RF}}^{\mathrm{r}}}$, $\mathcal{W} = \{\frac{1}{\sqrt{N_{\mathrm{r}}}} e^{j\frac{2\pi i}{2^b}} | i = 0, 1, \ldots, 2^b - 1\}$ and *ii)* there is only one nonzero element in each row, i.e. $\|\mathbf{W}_{\mathrm{RF}}(m,:)\|_0 = 1, m = 1, \ldots, N_{\mathrm{r}}$. Then the received signal is down-converted to baseband through $N_{\mathrm{RF}}^{\mathrm{r}}$ RF chains. After removing the cyclic prefix and applying the DFT, the received frequency-domain signal on each subcarrier is further processed by an individual digital combiner $\mathbf{W}_{\mathrm{BB},i} \in \mathbb{C}^{N_{\mathrm{RF}}^{\mathrm{r}} \times N_{\mathrm{s}}}, i = 1, \ldots, N_{\mathrm{F}}$, which yields the final processed signal at the i-th subcarrier as

$$\widehat{\mathbf{s}}_i = \mathbf{W}_{\mathrm{BB},i}^H \mathbf{W}_{\mathrm{RF}}^H \mathbf{H}_i \mathbf{F}_{\mathrm{RF}} \mathbf{F}_{\mathrm{BB},i} \mathbf{s}_i + \mathbf{W}_{\mathrm{BB},i}^H \mathbf{W}_{\mathrm{RF}}^H \mathbf{n}_i, \quad \forall i, \qquad (1)$$

where $\mathbf{H}_i \in \mathbb{C}^{N_{\mathrm{r}} \times N_{\mathrm{t}}}, i = 1, \ldots, N_{\mathrm{F}}$, denotes the channel at the i-th subcarrier, and $\mathbf{n}_i \sim \mathcal{CN}\left(\mathbf{0}, \sigma_i^2 \mathbf{I}_{N_{\mathrm{r}}}\right), i = 1, \ldots, N_{\mathrm{F}}$, is independently and identically distributed (i.i.d.) complex Gaussian noise.

B. Channel Model

1) Beam Squint Effect: In the wideband mmWave MIMO-OFDM system considered here, a common analog beamformer is applied over all subcarriers, even though the directional response of the beamformer will change with frequency. Thus, the beampattern will have a variation with θ for different subcarriers, and this effect is referred to as beam squint [40]. Fig. 2 illustrates an example of the resulting beampatterns as a function of θ for different frequencies. We can observe from Fig. 2 that, if we use a beamformer directed at angle $\theta_0 = \pi/3$ at carrier frequency $f_c = 60$GHz, the beamforming focus angles for other frequencies squint away from $\pi/3$, which illustrates the severe beamforming gain variations due to the beam squint effect. It is worth noting that beam squint is an inherent phenomenon that automatically appears in wideband mmWave channels since the array response vector is frequency-dependent. Therefore, it is necessary to take beam squint into consideration and provide an accurate model of the wideband mmWave MIMO-OFDM channel for the development of the hybrid beamformer design.

2) Wideband Channel Model With Beam Squint: Based on the discussions in [38]–[40], the beam squint effect is essentially induced by the frequency-dependent beam steering vectors. We first adopt the classical geometric channel model for mmWave MIMO systems, which can be described as a sum of the contributions of multiple propagation paths [3], [6], [11], [45]. The modified delay-d channel matrix can be written as [36]

$$\mathbf{H}[d] = \sum_{l=1}^{L} \alpha_l r(dT_{\mathrm{s}} - \tau_l) \mathbf{a}_{\mathrm{r}}(\phi_l^{\mathrm{r}}, \theta_l^{\mathrm{r}}, f) \mathbf{a}_{\mathrm{t}}^H(\phi_l^{\mathrm{t}}, \theta_l^{\mathrm{t}}, f), \quad \forall d, \qquad (2)$$

where L is the number of distinct scattering clusters and $\alpha_l \sim \mathcal{CN}(0,1)$ is the complex gain of the l-th cluster, $r(\tau)$ denotes the raised cosine pulse at τ, T_s is the sampling period and $\tau_l \in \mathbb{R}$ is the delay of the l-th cluster. The transmit/receive steering vector on frequency f of the l-th path with azimuth and elevation AoD/AOA of ϕ_l and θ_l is denoted as $\mathbf{a}(\phi_l, \theta_l, f)$. For an $N_{\mathrm{x}} \times N_{\mathrm{y}}$ UPA with N total antennas, the modified steering vector of the l-th cluster is given by [18]

$$\mathbf{a}(\phi_l, \theta_l, f) = \mathbf{a}_{\mathrm{x}}(\phi_l, \theta_l, f) \otimes \mathbf{a}_{\mathrm{y}}(\theta_l, f), \quad \forall l, \qquad (3)$$

where $\otimes$ is the Kronecker-product operation. The frequency-varying elevation steering vector $\mathbf{a}_{\mathrm{y}}(\theta_l, f)$ of the l-th cluster is

$$\mathbf{a}_{\mathrm{y}}(\theta_l, f) = [1, e^{j\pi \frac{f}{f_c} \cos\theta_l}, \ldots, e^{j(N_{\mathrm{y}}-1)\pi \frac{f}{f_c} \cos\theta_l}]^T, \quad \forall l. \qquad (4)$$

The frequency-varying azimuth steering vector $\mathbf{a}_{\mathrm{x}}(\phi_l, \theta_l, f)$ of the i-th cluster is given by

$$\mathbf{a}_{\mathrm{x}}(\phi_l, \theta_l, f) = [1, e^{j\pi \frac{f}{f_c} \sin\theta_l \sin\phi_l}, \ldots, e^{j(N_{\mathrm{x}}-1)\pi \frac{f}{f_c} \sin\theta_l \sin\phi_l}]^T, \quad \forall l. \qquad (5)$$

After the N_{F}-point DFT of the delay-domain channel $\mathbf{H}[d]$, the frequency-domain channel[1] at the i-th subcarrier, $i = 1, \ldots, N_{\mathrm{F}}$, can be expressed as

$$\mathbf{H}_i = \sum_{l=1}^{L} \alpha_l \beta_{\tau_l,i} \mathbf{a}_{\mathrm{r}}(\phi_l^{\mathrm{r}}, \theta_l^{\mathrm{r}}, f_i) \mathbf{a}_{\mathrm{t}}^H(\phi_l^{\mathrm{t}}, \theta_l^{\mathrm{t}}, f_i), \quad \forall i, \qquad (6)$$

where $\beta_{\tau_l,i}$ is defined as

$$\beta_{\tau_l,i} \triangleq \sum_{d=0}^{N_{\mathrm{F}}-1} r(dT_{\mathrm{s}} - \tau_l) e^{-j\frac{2\pi i d}{N_{\mathrm{F}}}}, \quad \forall i, l, \qquad (7)$$

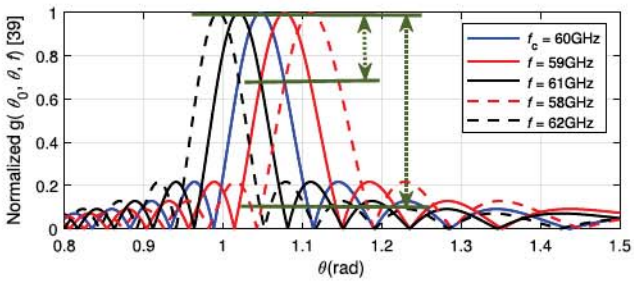

Fig. 2. Illustration of beam squint effect for a continuous-phase analog beamformer with one RF chain and M antennas described in [40] ($M = 64$ antennas, beamforming focus angle $\theta_0 = \pi/3$). At the angle of interest $\pi/3$, the beamforming gains of the $f = 59/61$GHz sub-bands will have a 30% degradation compared with that of carrier frequency $f_{\mathrm{c}} = 60$GHz. For a wider bandwidth, the $f = 58/62$GHz sub-bands will have very large 80% beamforming gain loss.

[1]In this paper, we assume that the channel $\mathbf{H}_i$ associated with each subcarrier is known to the transmitter based on the use of effective channel estimation algorithms [38], [39].

and f_i denotes the central frequency of the i-th subcarrier with total bandwidth B, which can be described as

$$f_i \triangleq f_{\mathrm{c}} + (i - \frac{N_{\mathrm{F}}+1}{2})\frac{B}{N_{\mathrm{F}}}, \quad \forall i. \tag{8}$$

C. Problem Formulation

With the mmWave MIMO-OFDM channel $\mathbf{H}_i$ in (6), the spectral efficiency of the i-th subcarrier is given by

$$R_i = \log(|\mathbf{I}_{N_{\mathrm{s}}} + \Upsilon_i^{-1}\mathbf{W}_{\mathrm{BB},i}^H\mathbf{W}_{\mathrm{RF}}^H\mathbf{H}_i\mathbf{F}_{\mathrm{RF}}\mathbf{F}_{\mathrm{BB},i} \times \mathbf{F}_{\mathrm{BB},i}^H\mathbf{F}_{\mathrm{RF}}^H\mathbf{H}_i^H\mathbf{W}_{\mathrm{RF}}\mathbf{W}_{\mathrm{BB},i}|), \quad \forall i, \tag{9}$$

where $\Upsilon_i \triangleq \sigma_i^2\mathbf{W}_{\mathrm{BB},i}^H\mathbf{W}_{\mathrm{RF}}^H\mathbf{W}_{\mathrm{RF}}\mathbf{W}_{\mathrm{BB},i}$ is the noise covariance matrix at the i-th subcarrier.

We aim to design the dynamic hybrid precoder and combiner as shown in Fig. 1 to maximize the average spectral efficiency over all subcarriers of the point-to-point MIMO-OFDM system, subject to the following constraints: *i)* Constant amplitude and discrete phase of PSs at the transmitter/receiver, i.e. $\mathbf{F}_{\mathrm{RF}}(m,k) \in \{\mathcal{F}, 0\}, m = 1,\ldots,N_{\mathrm{t}}, k = 1,\ldots,N_{\mathrm{RF}}^{\mathrm{t}}$, and $\mathbf{W}_{\mathrm{RF}}(m,k) \in \{\mathcal{W}, 0\}, m = 1,\ldots,N_{\mathrm{r}}, k = 1,\ldots,N_{\mathrm{RF}}^{\mathrm{r}}$; *ii)* the dynamic mapping, i.e. $\|\mathbf{F}_{\mathrm{RF}}(m,:)\|_0 = 1, m = 1,\ldots,N_{\mathrm{t}}$, and $\|\mathbf{W}_{\mathrm{RF}}(m,:)\|_0 = 1, m = 1,\ldots,N_{\mathrm{r}}$; *iii)* total transmit power constraint for all subcarriers, i.e. $\sum_{i=1}^{N_{\mathrm{F}}}\|\mathbf{F}_{\mathrm{RF}}\mathbf{F}_{\mathrm{BB},i}\|_F^2 \le P$, where P is the transmit power. With the above constraints, the dynamic hybrid beamformer design problem can be formulated as

$$\max_{\substack{\mathbf{F}_{\mathrm{RF}},\{\mathbf{F}_{\mathrm{BB},i}\}_{i=1}^{N_{\mathrm{F}}} \\ \mathbf{W}_{\mathrm{RF}},\{\mathbf{W}_{\mathrm{BB},i}\}_{i=1}^{N_{\mathrm{F}}}}} \frac{1}{N_{\mathrm{F}}}\sum_{i=1}^{N_{\mathrm{F}}} R_i \tag{10a}$$

$$\text{s.t. } \mathbf{F}_{\mathrm{RF}}(m,k) \in \{\mathcal{F}, 0\}, \quad \forall m,k, \tag{10b}$$

$$\|\mathbf{F}_{\mathrm{RF}}(m,:)\|_0 = 1, \quad \forall m, \tag{10c}$$

$$\mathbf{W}_{\mathrm{RF}}(m,k) \in \{\mathcal{W}, 0\}, \quad \forall m,k, \tag{10d}$$

$$\|\mathbf{W}_{\mathrm{RF}}(m,:)\|_0 = 1, \quad \forall m, \tag{10e}$$

$$\sum_{i=1}^{N_{\mathrm{F}}}\|\mathbf{F}_{\mathrm{RF}}\mathbf{F}_{\mathrm{BB},i}\|_F^2 \le P. \tag{10f}$$

Unfortunately, the hybrid beamformer design problem (10) is extremely difficult to solve due to not only the non-convex constraints of the analog beamformers but also the coupling of the digital/analog beamformers. To efficiently solve the problem (10), in the next section, we first transform the original problem into an alternative solvable form and then iteratively design the hybrid precoder and combiner.

III. Hybrid Precoder and Combiner Design

A. Problem Transformation

To tackle the difficulty arising from the spectral efficiency function of the optimization problem (10), i.e. the $\log(|\cdot|)$ function in (9), we first build a relationship between average spectral efficiency maximization and weighted MSE minimization [46][2] using the following proposition.

[2]Although this kind of method has been widely used for various optimization problems, in this paper we consider a different problem with a more complicated objective and additional non-convex constraints.

Proposition 1: Define the MSE matrix function as

$$\mathsf{E}_i \triangleq \mathbb{E}\{(\widehat{\mathbf{s}}_i - \mathbf{s}_i)(\widehat{\mathbf{s}}_i - \mathbf{s}_i)^H\} \tag{11a}$$

$$= \mathbf{W}_{\mathrm{BB},i}^H\mathbf{W}_{\mathrm{RF}}^H\mathbf{H}_i\mathbf{F}_{\mathrm{RF}}\mathbf{F}_{\mathrm{BB},i}\mathbf{F}_{\mathrm{BB},i}^H\mathbf{F}_{\mathrm{RF}}^H\mathbf{H}_i^H\mathbf{W}_{\mathrm{RF}}\mathbf{W}_{\mathrm{BB},i} - 2\Re\{\mathbf{W}_{\mathrm{BB},i}^H\mathbf{W}_{\mathrm{RF}}^H\mathbf{H}_i\mathbf{F}_{\mathrm{RF}}\mathbf{F}_{\mathrm{BB},i}\} + \mathbf{W}_{\mathrm{BB},i}^H\mathbf{W}_{\mathrm{RF}}^H\mathbf{W}_{\mathrm{RF}}\mathbf{W}_{\mathrm{BB},i}\sigma_i^2 + \mathbf{I}_{N_{\mathrm{s}}}, \quad \forall i. \tag{11b}$$

By introducing auxiliary weighting matrices $\mathbf{M}_i, i = 1,\ldots,N_{\mathrm{F}}$, the average spectral efficiency maximization problem (10) can be transformed into the following weighted MSE minimization problem

$$\max_{\substack{\mathbf{F}_{\mathrm{RF}},\{\mathbf{F}_{\mathrm{BB},i}\}_{i=1}^{N_{\mathrm{F}}}, \\ \mathbf{W}_{\mathrm{RF}},\{\mathbf{W}_{\mathrm{BB},i},\mathbf{M}_i\}_{i=1}^{N_{\mathrm{F}}}}} \frac{1}{N_{\mathrm{F}}}\sum_{i=1}^{N_{\mathrm{F}}}(\log(|\mathbf{M}_i|) - \mathrm{Tr}\{\mathbf{M}_i\mathsf{E}_i\} + N_s) \quad \text{s.t. (10b)} - \text{(10f)}, \tag{12}$$

where $\mathbf{M}_i \in \mathbb{C}^{N_{\mathrm{s}}\times N_{\mathrm{s}}}, i = 1,\ldots,N_{\mathrm{F}}$, is the auxiliary weighting matrix for the i-th subcarrier.

Proof: See Appendix A. ∎

Problem (12) is now more tractable than problem (10) since the complicated $\log(|\cdot|)$ function with multiple variables is removed. Instead, in problem (12) the $\log(|\cdot|)$ function is only with respect to the weighting matrix $\mathbf{M}_i$ and the sub-problem for solving $\mathbf{M}_i$ is a convex unconstrained optimization (see Sec. III-B for more details). For this kind of multi-variable-optimization problem, the classical block coordination descent (BCD) algorithms [47] have been widely used to decompose the original problem into several sub-problems to update each variable in a random order until convergence. However, when there are coupling constraints for different variables, the BCD algorithm cannot be directly applied. Moreover, the sub-problems with respect to the analog precoder/combiner are difficult to solve since the analog beamformers must be designed for all subcarriers with a complicated objective function subject to non-convex constraints (10b)-(10e). To facilitate the use of the BCD algorithm and simplify the analog beamformer design, we first introduce two auxiliary matrices $\mathbf{X}_i, \mathbf{Y}_i$, $i = 1,\ldots,N_{\mathrm{F}}$, for each subcarrier and then add them as coupling constraints (13b) and (13c) to problem (12):

$$\max_{\substack{\mathbf{F}_{\mathrm{RF}},\mathbf{W}_{\mathrm{RF}},\{\mathbf{M}_i\}_{i=1}^{N_{\mathrm{F}}} \\ \{\mathbf{X}_i,\mathbf{F}_{\mathrm{BB},i}\}_{i=1}^{N_{\mathrm{F}}}, \\ \{\mathbf{Y}_i,\mathbf{W}_{\mathrm{BB},i}\}_{i=1}^{N_{\mathrm{F}}}}} \frac{1}{N_{\mathrm{F}}}\sum_{i=1}^{N_{\mathrm{F}}}(\log(|\mathbf{M}_i|) - \mathrm{Tr}\{\mathbf{M}_i\widetilde{\mathsf{E}}_i\} + N_s) \tag{13a}$$

$$\text{s.t. } \mathbf{X}_i = \mathbf{F}_{\mathrm{RF}}\mathbf{F}_{\mathrm{BB},i}, \quad \forall i, \tag{13b}$$

$$\mathbf{Y}_i = \mathbf{W}_{\mathrm{RF}}\mathbf{W}_{\mathrm{BB},i}, \quad \forall i, \tag{13c}$$

$$\sum_{i=1}^{N_{\mathrm{F}}}\|\mathbf{X}_i\|_F^2 \le P, \tag{13d}$$

$$\text{(10b)} - \text{(10e)}, \tag{13e}$$

where the modified MSE matrix $\widetilde{\mathsf{E}}_i$ is defined as

$$\widetilde{\mathsf{E}}_i \triangleq \mathbf{Y}_i^H\mathbf{H}_i\mathbf{X}_i\mathbf{X}_i^H\mathbf{H}_i^H\mathbf{Y}_i - 2\Re\{\mathbf{Y}_i^H\mathbf{H}_i\mathbf{X}_i\} + \mathbf{Y}_i^H\mathbf{Y}_i\sigma_i^2 + \mathbf{I}_{N_{\mathrm{s}}}, \quad \forall i. \tag{14}$$

Inspired by [48] which proposed a penalty dual decomposition (PDD) algorithm to simplify the coupling constraints with an appropriate penalty term, we also introduce two penalty terms $\frac{1}{2\rho_{\mathrm{t}}}\|\mathbf{X}_i-\mathbf{F}_{\mathrm{RF}}\mathbf{F}_{\mathrm{BB},i}\|_F^2$ and $\frac{1}{2\rho_{\mathrm{r}}}\|\mathbf{Y}_i-\mathbf{W}_{\mathrm{RF}}\mathbf{W}_{\mathrm{BB},i}\|_F^2$ associated with the equality constraints (13b) and (13c), respectively, where ρ_{t} and ρ_{r} are two penalty parameters. Then, the penalty terms are added to the objective function and problem (13) is reformulated as problem (15) shown at the bottom of this page. Now the constraints for each variable are separated and the BCD algorithm can be utilized to iteratively solve for the variables $\{\mathbf{M}_i\}_{i=1}^{N_{\mathrm{F}}}$, $\mathbf{F}_{\mathrm{RF}}$, $\{\mathbf{F}_{\mathrm{BB},i}\}_{i=1}^{N_{\mathrm{F}}}$, $\{\mathbf{X}_i\}_{i=1}^{N_{\mathrm{F}}}$, $\mathbf{W}_{\mathrm{RF}}$, $\{\mathbf{W}_{\mathrm{BB},i}\}_{i=1}^{N_{\mathrm{F}}}$, $\{\mathbf{Y}_i\}_{i=1}^{N_{\mathrm{F}}}$. In the following subsection, we will discuss the solution for each block in detail.

B. Block Update

1) Block $\{\boldsymbol{M}_i\}_{i=1}^{N_{\mathrm{F}}}$: Under fixed beamformers and other auxiliary variables $\mathbf{X}_i, \mathbf{Y}_i$, the sub-problem with respect to $\mathbf{M}_i, i=1,\ldots,N_{\mathrm{F}}$, is a convex unconstrained problem, i.e.

$$\max_{\mathbf{M}_i} \quad \log(|\mathbf{M}_i|)-\mathrm{Tr}\{\mathbf{M}_i\widetilde{\mathbf{E}}_i\}, \quad \forall i. \tag{16}$$

Thus, the optimal $\mathbf{M}_i^\star$ can be obtained by setting the partial derivative of the objective in (16) with respect to $\mathbf{M}_i$ to zero, which yields the following optimal value:

$$\mathbf{M}_i^\star=\widetilde{\mathbf{E}}_i^{-1}=[\mathbf{Y}_i^H\widetilde{\mathbf{A}}_i\mathbf{Y}_i-2\Re\{\mathbf{Y}_i^H\mathbf{H}_i\mathbf{X}_i\}+\mathbf{I}_{N_{\mathrm{s}}}]^{-1}, \quad \forall i, \tag{17}$$

where

$$\widetilde{\mathbf{A}}_i\triangleq\mathbf{H}_i\mathbf{X}_i\mathbf{X}_i^H\mathbf{H}_i^H+\sigma_i^2\mathbf{I}, \quad \forall i. \tag{18}$$

2) Block $\{\boldsymbol{X}_i\}_{i=1}^{N_{\mathrm{F}}}$: With given beamformers and weighting matrix $\mathbf{M}_i$, the sub-problem with respect to $\mathbf{X}_i$ is given by

$$\min_{\{\mathbf{X}_i\}_{i=1}^{N_{\mathrm{F}}}} \sum_{i=1}^{N_{\mathrm{F}}}\left(\mathrm{Tr}\{\mathbf{M}_i\widetilde{\mathbf{E}}_i\}+\frac{1}{2\rho_{\mathrm{t}}}\|\mathbf{X}_i-\mathbf{F}_{\mathrm{RF}}\mathbf{F}_{\mathrm{BB},i}\|_F^2\right)$$
$$\text{s.t.} \sum_{i=1}^{N_{\mathrm{F}}}\|\mathbf{X}_i\|_F^2\le P. \tag{19}$$

The optimal solution of (19) can be determined by the Lagrange multiplier method. By introducing a multiplier $\mu\ge 0$ for the power constraint (13d), we can form a Lagrangian function to transform the problem (19) into an unconstrained optimization as

$$\min_{\mu,\{\mathbf{X}_i\}_{i=1}^{N_{\mathrm{F}}}} \sum_{i=1}^{N_{\mathrm{F}}}\left(\mathrm{Tr}\{\mathbf{M}_i\widetilde{\mathbf{E}}_i\}+\frac{1}{2\rho_{\mathrm{t}}}\|\mathbf{X}_i-\mathbf{F}_{\mathrm{RF}}\mathbf{F}_{\mathrm{BB},i}\|_F^2\right)$$
$$+\mu\left(\sum_{i=1}^{N_{\mathrm{F}}}\|\mathbf{X}_i\|_F^2-P\right). \tag{20}$$

Then, the optimal $\mathbf{X}_i, i=1,\ldots,N_{\mathrm{F}}$, can be determined by setting the partial derivative of the objective in (20) with respect to $\mathbf{X}_i$ and μ to zero, which yields the optimal solution as

$$\mathbf{X}_i^\star=(\mathbf{H}_i^H\mathbf{Y}_i\mathbf{M}_i\mathbf{Y}_i^H\mathbf{H}_i+\frac{1}{2\rho_{\mathrm{t}}}\mathbf{I}+\mu\mathbf{I})^{-1}$$
$$\times(\mathbf{H}_i^H\mathbf{Y}_i\mathbf{M}_i+\frac{1}{2\rho_{\mathrm{t}}}\mathbf{F}_{\mathrm{RF}}\mathbf{F}_{\mathrm{BB},i}), \quad \forall i, \tag{21}$$

where the optimal multiplier μ is associated with total power constraint, i.e. $\sum_{i=1}^{N_{\mathrm{F}}}\|\mathbf{X}_i^\star\|_F^2\le P$.

To determine the value of μ, we begin by analyzing the term $\sum_{i=1}^{N_{\mathrm{F}}}\|\mathbf{X}_i^\star\|_F^2$. We first rewrite it as

$$\sum_{i=1}^{N_{\mathrm{F}}}\|\mathbf{X}_i^\star\|_F^2=\sum_{i=1}^{N_{\mathrm{F}}}\mathrm{Tr}\{(\mathbf{X}_i^\star)^H\mathbf{X}_i^\star\} \tag{22a}$$
$$=\sum_{i=1}^{N_{\mathrm{F}}}\mathrm{Tr}\{(\mathbf{H}_i^H\mathbf{Y}_i\mathbf{M}_i+\frac{1}{2\rho_{\mathrm{t}}}\mathbf{F}_{\mathrm{RF}}\mathbf{F}_{\mathrm{BB},i})^H$$
$$\times(\mathbf{H}_i^H\mathbf{Y}_i\mathbf{M}_i\mathbf{Y}_i^H\mathbf{H}_i+\frac{1}{2\rho_{\mathrm{t}}}\mathbf{I}+\mu\mathbf{I})^{-2}$$
$$\times(\mathbf{H}_i^H\mathbf{Y}_i\mathbf{M}_i+\frac{1}{2\rho_{\mathrm{t}}}\mathbf{F}_{\mathrm{RF}}\mathbf{F}_{\mathrm{BB},i})\}. \tag{22b}$$

We define $\mathbf{P}_i\triangleq(\mathbf{H}_i^H\mathbf{Y}_i\mathbf{M}_i+\frac{1}{2\rho_{\mathrm{t}}}\mathbf{F}_{\mathrm{RF}}\mathbf{F}_{\mathrm{BB},i})(\mathbf{H}_i^H\mathbf{Y}_i\mathbf{M}_i+\frac{1}{2\rho_{\mathrm{t}}}\mathbf{F}_{\mathrm{RF}}\mathbf{F}_{\mathrm{BB},i})^H$ and $\mathbf{Q}_i\triangleq\mathbf{H}_i^H\mathbf{Y}_i\mathbf{M}_i\mathbf{Y}_i^H\mathbf{H}_i$ for each subcarrier, then the above equation is further rewritten as

$$\sum_{i=1}^{N_{\mathrm{F}}}\|\mathbf{X}_i^\star\|_F^2=\sum_{i=1}^{N_{\mathrm{F}}}\mathrm{Tr}\{(\mathbf{Q}_i+\frac{1}{2\rho_{\mathrm{t}}}\mathbf{I}+\mu\mathbf{I})^{-2}\mathbf{P}_i\}, \tag{23a}$$
$$\overset{(a)}{=}\sum_{i=1}^{N_{\mathrm{F}}}\mathrm{Tr}\{(\mathbf{U}_i\mathbf{\Xi}_i\mathbf{U}_i^H+\frac{1}{2\rho_{\mathrm{t}}}\mathbf{I}+\mu\mathbf{I})^{-2}\mathbf{P}_i\}, \tag{23b}$$
$$\overset{(b)}{=}\sum_{i=1}^{N_{\mathrm{F}}}\mathrm{Tr}\{(\mathbf{\Xi}_i+\frac{1}{2\rho_{\mathrm{t}}}\mathbf{I}+\mu\mathbf{I})^{-2}\overline{\mathbf{P}}_i\}, \tag{23c}$$
$$\overset{(c)}{=}\sum_{i=1}^{N_{\mathrm{F}}}\sum_{j=1}^{N_{\mathrm{t}}}\frac{p_{i,j}}{(\varepsilon_{i,j}+\frac{1}{2\rho_{\mathrm{t}}}+\mu)^2}, \tag{23d}$$

where (a) holds by performing the eigenvalue decomposition (EVD) $\mathbf{Q}_i\triangleq\mathbf{U}_i\mathbf{\Xi}\mathbf{U}_i^H, i=1,\ldots,N_{\mathrm{F}}$; (b) holds by defining $\overline{\mathbf{P}}_i\triangleq\mathbf{U}_i^H\mathbf{P}_i\mathbf{U}_i$ for each subcarrier; finally, (c) holds by denoting $\varepsilon_{i,j}$ as the (j,j)-th element of the matrix $\mathbf{\Xi}_i$ and $p_{i,j}$ as the (j,j)-th element of the matrix $\overline{\mathbf{P}}_i$. Therefore, it can be shown that $\sum_{i=1}^{N_{\mathrm{F}}}\|\mathbf{X}_i^\star\|_F^2$ is a monotonically decreasing function with respect to μ. When $\mu\to 0$, we can obtain the following upper bound, i.e.

$$\lim_{\mu\to 0}\sum_{i=1}^{N_{\mathrm{F}}}\|\mathbf{X}_i^\star\|_F^2=\sum_{i=1}^{N_{\mathrm{F}}}\sum_{j=1}^{N_{\mathrm{t}}}\frac{p_{i,j}}{(\varepsilon_{i,j}+\frac{1}{2\rho_{\mathrm{t}}})^2}. \tag{24}$$

With this upper bound, we can obtain the optimal value of $\mathbf{X}_i$ under the following two conditions:

$$\max_{\substack{\mathbf{F}_{\mathrm{RF}},\mathbf{W}_{\mathrm{RF}},\{\mathbf{M}_i\}_{i=1}^{N_{\mathrm{F}}}\\ \{\mathbf{X}_i,\mathbf{F}_{\mathrm{BB},i}\}_{i=1}^{N_{\mathrm{F}}},\{\mathbf{Y}_i,\mathbf{W}_{\mathrm{BB},i}\}_{i=1}^{N_{\mathrm{F}}}}} \frac{1}{N_{\mathrm{F}}}\sum_{i=1}^{N_{\mathrm{F}}}\left(\log(|\mathbf{M}_i|)-\mathrm{Tr}\{\mathbf{M}_i\widetilde{\mathbf{E}}_i\}-\frac{1}{2\rho_{\mathrm{t}}}\|\mathbf{X}_i-\mathbf{F}_{\mathrm{RF}}\mathbf{F}_{\mathrm{BB},i}\|_F^2-\frac{1}{2\rho_{\mathrm{r}}}\|\mathbf{Y}_i-\mathbf{W}_{\mathrm{RF}}\mathbf{W}_{\mathrm{BB},i}\|_F^2\right), \tag{15a}$$

$$\text{s.t.} \quad (10\text{b})-(10\text{e}),(13\text{d}) \tag{15b}$$

C1: When the upper bound $\sum_{i=1}^{N_\mathrm{F}}\sum_{j=1}^{N_\mathrm{t}}\frac{p_{i,j}}{(\varepsilon_{i,j}+\frac{1}{2\rho_\mathrm{t}})^2} \le P$, which means the power constraint is satisfied for all $\mu \ge 0$, we can directly obtain the optimal value of $\mathbf{X}_i$ by setting $\mu = 0$ as

$$\mathbf{X}_i^\star = (\mathbf{H}_i^H\mathbf{Y}_i\mathbf{M}_i\mathbf{Y}_i^H\mathbf{H}_i + \frac{1}{2\rho_\mathrm{t}}\mathbf{I})^{-1} \times (\mathbf{H}_i^H\mathbf{Y}_i\mathbf{M}_i + \frac{1}{2\rho_\mathrm{t}}\mathbf{F}_\mathrm{RF}\mathbf{F}_{\mathrm{BB},i}), \quad \forall i. \tag{25}$$

C2: When the upper bound $\sum_{i=1}^{N_\mathrm{F}}\sum_{j=1}^{N_\mathrm{t}}\frac{p_{i,j}}{(\varepsilon_{i,j}+\frac{1}{2\rho_\mathrm{t}})^2} > P$, the optimal multiplier μ can be easily found by a bisection search over the set

$$\mathcal{S}_\mu \triangleq \{\mu \in \mathbb{R}^+ \mid \sum_{i=1}^{N_\mathrm{F}} \|\mathbf{X}_i^\star\|_F^2 = P\}. \tag{26}$$

3) Block $\{\boldsymbol{F}_{\mathrm{BB},i}\}_{i=1}^{N_F}$: When the analog precoder $\mathbf{F}_\mathrm{RF}$, overall hybrid combiner $\mathbf{W}_i$, auxiliary variables $\mathbf{X}_i$, $\mathbf{Y}_i$ and $\mathbf{M}_i$ are all fixed, $\mathbf{F}_{\mathrm{BB},i}, i = 1,\ldots,N_\mathrm{F}$, only appears in the second term of the objective (15a). In this case, the sub-problem with respect to $\mathbf{F}_{\mathrm{BB},i}$ can be formulated as an unconstrained problem, i.e.

$$\min_{\mathbf{F}_{\mathrm{BB},i}} \ \|\mathbf{X}_i - \mathbf{F}_\mathrm{RF}\mathbf{F}_{\mathrm{BB},i}\|_F^2, \quad \forall i. \tag{27}$$

Then we can easily obtain the optimal solution of the above least squares problem as

$$\mathbf{F}_{\mathrm{BB},i}^\star = \mathbf{F}_\mathrm{RF}^\dagger\mathbf{X}_i, \quad \forall i. \tag{28}$$

4) Block $\boldsymbol{F}_{RF}$: The analog precoder $\mathbf{F}_\mathrm{RF}$ appears only in the second term of the objective (15a) with other fixed blocks. Therefore, the sub-problem with respect to $\mathbf{F}_\mathrm{RF}$ is given by[3]

$$\min_{\mathbf{F}_\mathrm{RF}} \ \sum_{i=1}^{N_\mathrm{F}} \|\mathbf{X}_i - \mathbf{F}_\mathrm{RF}\mathbf{F}_{\mathrm{BB},i}\|_F^2 \tag{29a}$$

$$\text{s.t. } \mathbf{F}_\mathrm{RF}(m,k) \in \{\mathcal{F}, 0\}, \quad \forall m,k, \tag{29b}$$

$$\|\mathbf{F}_\mathrm{RF}(m,:)\|_0 = 1, \quad \forall m. \tag{29c}$$

Defining $\widetilde{\mathbf{X}} \triangleq [\mathbf{X}_1,\ldots,\mathbf{X}_{N_\mathrm{F}}]$, $\widetilde{\mathbf{F}}_\mathrm{BB} \triangleq [\mathbf{F}_{\mathrm{BB},1},\ldots,\mathbf{F}_{\mathrm{BB},N_\mathrm{F}}]$, the objective $\sum_{i=1}^{N_\mathrm{F}}\|\mathbf{X}_i - \mathbf{F}_\mathrm{RF}\mathbf{F}_{\mathrm{BB},i}\|_F^2$ can be rewritten as $\|\widetilde{\mathbf{X}} - \mathbf{F}_\mathrm{RF}\widetilde{\mathbf{F}}_\mathrm{BB}\|_F^2$. Since there is only one nonzero element with constant magnitude and discrete phase in each row of the analog precoder, the above least squares problem can be split apart row-by-row and the nonzero element at each row can be separately determined. Based on this observation, we can further simplify the objective function using the following proposition.

Proposition 2: Let $\mathcal{D}_m^\mathrm{t}, m = 1,\ldots,N_\mathrm{RF}^\mathrm{t}$ be N_RF^t disjoint subsets which store the indices of the transmit antennas connected to each RF chain. With these subsets, the constraint (29c) of the analog precoder can be redescribed as

$$\cup_{m=1}^{N_\mathrm{RF}^\mathrm{t}}\mathcal{D}_m^\mathrm{t} = \mathcal{N}_\mathrm{t} \triangleq \{1,\ldots,N_\mathrm{t}\}, \tag{30a}$$

$$\mathcal{D}_p^\mathrm{t} \cap \mathcal{D}_q^\mathrm{t} = \varnothing, \quad \forall p \ne q. \tag{30b}$$

[3]While Euclidean distance minimization is a typical approach, in this paper we consider different constraints and design a novel low-complexity algorithm.

Denote $\varpi_{m,n}^\mathrm{t} \triangleq \widetilde{\mathbf{F}}_\mathrm{BB}(m,:)\widetilde{\mathbf{X}}(n,:)^H$. Let $\zeta_{m,n}^\mathrm{t}$ be the angle of $\varpi_{m,n}^\mathrm{t}$, i.e. $\zeta_{m,n}^\mathrm{t} \triangleq \angle\varpi_{m,n}^\mathrm{t} \in (-\pi,\pi]$, $\xi_{m,n}^\mathrm{t}$ be the angle of the corresponding nonzero element of the analog precoder, i.e. $\xi_{m,n}^\mathrm{t} \triangleq \angle\mathbf{F}_\mathrm{RF}(n,m)$, and $\mathcal{B}$ be the set of discrete phases of the low-resolution PSs, i.e. $\mathcal{B} \triangleq \{\frac{2\pi i}{2^b} | i = 0,1,\ldots,2^b-1\}$. Then, problem (29) can be transformed to

$$\max_{\substack{\{\xi_{m,n}^\mathrm{t},\forall m,n\}\\ \{\mathcal{D}_m^\mathrm{t}\}_{m=1}^{N_\mathrm{RF}^\mathrm{t}}}} \ \sum_{m=1}^{N_\mathrm{RF}^\mathrm{t}}\sum_{n\in\mathcal{D}_m^\mathrm{t}} |\varpi_{m,n}^\mathrm{t}|\cos(\zeta_{m,n}^\mathrm{t} + \xi_{m,n}^\mathrm{t}) \tag{31a}$$

$$\text{s.t. } (30a), (30b), \tag{31b}$$

$$\xi_{m,n}^\mathrm{t} \in \mathcal{B}, \quad \forall m,n. \tag{31c}$$

Proof: See Appendix B. ∎

Obviously, if $\xi_{m,n}^\mathrm{t}$ has continuous phase, the $\cos(\cdot)$ term can always achieve its maximum value, i.e. $\cos(0) = 1$, by letting $\xi_{m,n}^\mathrm{t} = -\zeta_{m,n}^\mathrm{t}$, and each dynamic subarray set can be easily determined by searching $|\varpi_{m,n}^\mathrm{t}|$ over all antennas. Although low-resolution PSs are employed in this paper (i.e. $\xi_{m,n}^\mathrm{t} \in \mathcal{B}$), this problem is still easy to solve by firstly finding the optimal value of $\cos(\zeta_{m,n}^\mathrm{t} + \xi_{m,n}^\mathrm{t})$ corresponding to $\varpi_{m,n}^\mathrm{t}$ for all RF chains and antennas, and then determining the optimal dynamic mapping subsets by one-dimensional exhaustive search. To efficiently solve this problem, we propose a simple two-step algorithm to optimally determine the analog precoder, which is illustrated as follows.

Step 1: Calculate the optimal phases of $\xi_{m,n}^\mathrm{t}, m = 1,\ldots,N_\mathrm{F}, n \in \mathcal{N}_\mathrm{t}$, by the quantization operation as

$$\widetilde{\xi}_{m,n}^\mathrm{t} = \begin{cases} [\frac{-\zeta_{m,n}^\mathrm{t}}{\Delta}] \times \Delta + 2\pi, & 0 < \zeta_{m,n}^\mathrm{t} \le \pi, \\ [\frac{-\zeta_{m,n}^\mathrm{t}}{\Delta}] \times \Delta, & -\pi < \zeta_{m,n}^\mathrm{t} \le 0. \end{cases} \tag{32}$$

where $[\cdot]$ denotes the rounding operation, $\Delta \triangleq 2\pi/2^b$ is the angle resolution.

Step 2: For each antenna n, map the antenna to the RF chain m that maximizes $|\varpi_{m,n}^\mathrm{t}|\cos(\zeta_{m,n}^\mathrm{t} + \widetilde{\xi}_{m,n}^\mathrm{t})$, i.e.

$$m_n^\star = \arg\max_m \ |\varpi_{m,n}^\mathrm{t}|\cos(\zeta_{m,n}^\mathrm{t} + \widetilde{\xi}_{m,n}^\mathrm{t}), \tag{33}$$

and update the corresponding dynamic subset for that RF chain:

$$\mathcal{D}_{m_n^\star}^\mathrm{t} = \mathcal{D}_{m_n^\star}^\mathrm{t} \cup \{n\}. \tag{34}$$

After performing (33) through all transmit antennas, we can obtain the optimal dynamic subarray sets and the corresponding optimal analog beamformer as

$$\mathbf{F}_\mathrm{RF}^\star(n,m) = \begin{cases} \frac{1}{\sqrt{N_\mathrm{t}}}e^{j\widetilde{\xi}_{m,n}^\mathrm{t}}, & n \in \mathcal{D}_m^\mathrm{t}, \\ 0, & \text{otherwise.} \end{cases} \tag{35}$$

Now the analog precoder design algorithm is completed and summarized in Algorithm 1. The optimality of Algorithm 1 is straightforward since each nonzero element of the analog precoder can be solved for separately via an exhaustive search.

Algorithm 1 Analog Precoder Design

Input: $\widetilde{\mathbf{X}}, \widetilde{\mathbf{F}}_{\mathrm{BB}}, \Delta$.
Output: $\mathbf{F}_{\mathrm{RF}}^{\star}$.
1: Initialize $\mathbf{F}_{\mathrm{RF}} = \mathbf{0}_{N_{\mathrm{t}} \times N_{\mathrm{RF}}^{\mathrm{t}}}$, $\mathcal{D}_1^{\mathrm{t}} = \ldots = \mathcal{D}_{N_{\mathrm{RF}}^{\mathrm{t}}}^{\mathrm{t}} = \varnothing$.
2: **for** $n = 1$: N_{t} **do**
3: **for** $m = 1$: $N_{\mathrm{RF}}^{\mathrm{t}}$ **do**
4: Calculate $\widetilde{\xi}_{m,n}^{\mathrm{t}}$ by (32).
5: **end for**
6: Map the n-th antenna to RF chain $m_n^{\star}$ by (33).
7: Update $\mathcal{D}_{m_n^{\star}}^{\mathrm{t}} = \mathcal{D}_{m_n^{\star}}^{\mathrm{t}} \cup \{n\}$.
8: **end for**
9: Obtain $\mathbf{F}_{\mathrm{RF}}^{\star}$ by (35).

5) Block $\{\mathbf{Y}_i\}_{i=1}^{N_{\mathrm{F}}}$: When other blocks are fixed, the sub-problem with respect to the variable $\mathbf{Y}_i$ can be formulated as

$$\min_{\mathbf{Y}_i} \quad \mathrm{Tr}\{\mathbf{M}_i \widetilde{\mathbf{E}}_i\} + \frac{1}{2\rho_{\mathrm{r}}} \|\mathbf{Y}_i - \mathbf{W}_{\mathrm{RF}} \mathbf{W}_{\mathrm{BB},i}\|_F^2, \quad \forall i. \tag{36}$$

By setting the partial derivative of the objective in (36) with respect to $\mathbf{Y}_i$ to zero, we have

$$\widetilde{\mathbf{A}}_i \mathbf{Y}_i \mathbf{M}_i + \frac{1}{2\rho_{\mathrm{r}}} \mathbf{Y}_i = \mathbf{H}_i \mathbf{X}_i \mathbf{M}_i + \frac{1}{2\rho_{\mathrm{r}}} \mathbf{W}_{\mathrm{RF}} \mathbf{W}_{\mathrm{BB},i}, \quad \forall i, \tag{37}$$

which is a typical Sylvester equation [49]. Using the Kronecker product $\otimes$ and vectorization operator $\mathrm{vec}(\cdot)$ which stacks the columns of a matrix into a vector, equation (37) can be rewritten as

$$(\mathbf{M}_i^T \otimes \widetilde{\mathbf{A}}_i + \mathbf{I}_{N_{\mathrm{s}}} \otimes \frac{1}{2\rho_{\mathrm{r}}} \mathbf{I}_{N_{\mathrm{r}}}) \widetilde{\mathbf{y}}_i = \widetilde{\mathbf{x}}_i, \quad \forall i, \tag{38}$$

where $\widetilde{\mathbf{y}}_i \triangleq \mathrm{vec}(\mathbf{Y}_i)$, $\widetilde{\mathbf{x}}_i \triangleq \mathrm{vec}(\mathbf{H}_i \mathbf{X}_i \mathbf{M}_i + \frac{1}{2\rho_{\mathrm{r}}} \mathbf{W}_{\mathrm{RF}} \mathbf{W}_{\mathrm{BB},i})$. Therefore, the optimal solution for $\widetilde{\mathbf{y}}_i$ can be easily found by

$$\widetilde{\mathbf{y}}_i = (\mathbf{M}_i^T \otimes \widetilde{\mathbf{A}}_i + \mathbf{I}_{N_{\mathrm{s}}} \otimes \frac{1}{2\rho_{\mathrm{r}}} \mathbf{I}_{N_{\mathrm{r}}})^{-1} \widetilde{\mathbf{x}}_i, \quad \forall i. \tag{39}$$

After reshaping vector (39), we can obtain the optimal $\mathbf{Y}_i^{\star}$ as

$$\mathbf{Y}_i^{\star}(:, k) = \widetilde{\mathbf{y}}_i((k-1)N_{\mathrm{r}} + 1 : kN_{\mathrm{r}}), \quad \forall k, i. \tag{40}$$

6) Block $\{\boldsymbol{W}_{BB,i}\}_{i=1}^{N_F}$: Similar to the digital precoder design, when the other blocks are all fixed, $\mathbf{W}_{\mathrm{BB},i}$, $i = 1, \ldots, N_{\mathrm{F}}$, can be obtained by an unconstrained least squares problem, i.e.

$$\min_{\mathbf{W}_{\mathrm{BB},i}} \quad \|\mathbf{Y}_i - \mathbf{W}_{\mathrm{RF}} \mathbf{W}_{\mathrm{BB},i}\|_F^2, \quad \forall i, \tag{41}$$

which can be easily solved as

$$\mathbf{W}_{\mathrm{BB},i}^{\star} = \mathbf{W}_{\mathrm{RF}}^{\dagger} \mathbf{Y}_i, \quad \forall i. \tag{42}$$

7) Block $\boldsymbol{W}_{RF}$: With the other blocks fixed, the analog combiner matrix $\mathbf{W}_{\mathrm{RF}}$ appears only in the last term of the objective (15a). Therefore, the sub-problem with respect to $\mathbf{W}_{\mathrm{RF}}$ can be formulated as

$$\min_{\mathbf{W}_{\mathrm{RF}}} \quad \sum_{i=1}^{N_{\mathrm{F}}} \|\mathbf{Y}_i - \mathbf{W}_{\mathrm{RF}} \mathbf{W}_{\mathrm{BB},i}\|_F^2 \tag{43a}$$

$$\text{s.t. } \mathbf{W}_{\mathrm{RF}}(m,k) \in \{\mathcal{W}, 0\}, \quad \forall m, k, \tag{43b}$$

$$\|\mathbf{W}_{\mathrm{RF}}(m,:)\|_0 = 1, \quad \forall m, \tag{43c}$$

which has the same form as problem (29). Defining $\widetilde{\mathbf{Y}} \triangleq [\mathbf{Y}_1, \ldots, \mathbf{Y}_{N_{\mathrm{F}}}]$, $\widetilde{\mathbf{W}}_{\mathrm{BB}} \triangleq [\mathbf{W}_{\mathrm{BB},1}, \ldots, \mathbf{W}_{\mathrm{BB},N_{\mathrm{F}}}]$, and $N_{\mathrm{RF}}^{\mathrm{r}}$ disjoint subsets $\mathcal{D}_m^{\mathrm{r}}, m = 1, \ldots, N_{\mathrm{RF}}^{\mathrm{r}}$, which contain the indices of the receive antennas connected to each RF chain, problem (43) can be equivalently reformulated similar to Proposition 2 as

$$\max_{\substack{\{\xi_{m,n}^{\mathrm{r}}, \forall m,n\} \\ \{\mathcal{D}_m^{\mathrm{r}}\}_{m=1}^{N_{\mathrm{RF}}^{\mathrm{r}}}}} \quad \sum_{m=1}^{N_{\mathrm{RF}}^{\mathrm{r}}} \sum_{n \in \mathcal{D}_m^{\mathrm{r}}} |\varpi_{m,n}^{\mathrm{r}}| \cos(\zeta_{m,n}^{\mathrm{r}} + \xi_{m,n}^{\mathrm{r}}) \tag{44a}$$

$$\text{s.t. } \cup_{m=1}^{N_{\mathrm{RF}}^{\mathrm{r}}} \mathcal{D}_m^{\mathrm{r}} = \mathcal{N}_{\mathrm{r}} \triangleq \{1, \ldots, N_{\mathrm{r}}\}, \tag{44b}$$

$$\mathcal{D}_p^{\mathrm{r}} \cap \mathcal{D}_q^{\mathrm{r}} = \varnothing, \quad \forall p \neq q, \tag{44c}$$

$$\xi_{m,n}^{\mathrm{r}} \in \mathcal{B}, \quad \forall m, n. \tag{44d}$$

where $\varpi_{m,n}^{\mathrm{r}} \triangleq \widetilde{\mathbf{W}}_{\mathrm{BB}}(m,:) \widetilde{\mathbf{Y}}(n,:)^H$, $\zeta_{m,n}^{\mathrm{r}} \triangleq \angle \varpi_{m,n}^{\mathrm{r}} \in (-\pi, \pi]$, $\xi_{m,n}^{\mathrm{r}} \triangleq \angle \mathbf{W}_{\mathrm{RF}}(n,m)$. Problem (44) can be solved by the same method as in Algorithm 1.

8) Summary: With methods now for finding the conditionally optimal block variables $\{\mathbf{M}_i\}_{i=1}^{N_{\mathrm{F}}}$, $\mathbf{F}_{\mathrm{RF}}$, $\{\mathbf{F}_{\mathrm{BB},i}\}_{i=1}^{N_{\mathrm{F}}}$, $\{\mathbf{X}_i\}_{i=1}^{N_{\mathrm{F}}}$, $\mathbf{W}_{\mathrm{RF}}$, $\{\mathbf{W}_{\mathrm{BB},i}\}_{i=1}^{N_{\mathrm{F}}}$, $\{\mathbf{Y}_i\}_{i=1}^{N_{\mathrm{F}}}$, the overall procedure for the proposed hybrid beamformer design is now straightforward. With appropriate initial values, we iteratively update the above blocks until convergence. Since we do not update the two penalty parameters[4] $\rho_{\mathrm{t}}, \rho_{\mathrm{r}}$ in solving problem (15), the approximation of $\mathbf{F}_{\mathrm{RF}} \mathbf{F}_{\mathrm{BB},i}$ by the auxiliary matrix $\mathbf{X}_i$ for each subcarrier will not be exact, which may lead to a violation of the transmit power constraint. Thus, in the final step we perform a simple normalization for the digital precoders to ensure the transmit power constraint, i.e.

$$\mathbf{F}_{\mathrm{BB},i}^{\star} = \frac{\sqrt{P} \mathbf{F}_{\mathrm{BB},i}^{\star}}{\sqrt{\sum_{i=1}^{N_{\mathrm{F}}} \|\mathbf{F}_{\mathrm{RF}}^{\star} \mathbf{F}_{\mathrm{BB},i}^{\star}\|_F^2}}, \quad \forall i. \tag{45}$$

The proposed dynamic hybrid beamformer design algorithm is thus summarized in Algorithm 2.

C. Initialization

For Algorithm 2, an appropriate initialization for the hybrid precoders/combiners is needed. As this algorithm leads to a locally optimal solution, it is desirable to initialize beamformers that are "close" to the optimal solution. In this subsection, we provide an approach for designing an accurate initial value of the hybrid beamformers. For the analog precoder/combiner, we first define an average channel matrix $\widetilde{\mathbf{H}} \triangleq \frac{1}{N_{\mathrm{F}}} \sum_{i=1}^{N_{\mathrm{F}}} \mathbf{H}_i$, and then perform the singular value decomposition (SVD) $\widetilde{\mathbf{H}} = \widetilde{\mathbf{U}} \widetilde{\mathbf{\Sigma}} \widetilde{\mathbf{V}}^H$, where $\widetilde{\mathbf{U}}$ and $\widetilde{\mathbf{V}}$ are unitary matrices, and $\widetilde{\mathbf{\Sigma}}$ is a diagonal matrix of singular values. Here, we assume the fixed-subarray scheme and choose the $N_{\mathrm{RF}}^{\mathrm{t}}/N_{\mathrm{RF}}^{\mathrm{r}}$ strongest components as the initial value of the analog precoder/combiner, i.e.

$$\mathbf{F}_{\mathrm{RF}} = \mathrm{blkdiag}(\mathbf{f}_1, \ldots, \mathbf{f}_{N_{\mathrm{RF}}^{\mathrm{t}}}), \tag{46a}$$

$$\mathbf{f}_k = \frac{1}{\sqrt{N_{\mathrm{t}}}} e^{j\mathcal{Q}\{\angle \widetilde{\mathbf{V}}((k-1)N_{\mathrm{t}}/N_{\mathrm{RF}}^{\mathrm{t}} + 1 : kN_{\mathrm{t}}/N_{\mathrm{RF}}^{\mathrm{t}}, k)\}}, \quad \forall k, \tag{46b}$$

[4]Here the penalty parameters are fixed and are not be updated in order to maintain low complexity; this results in a negligible performance loss.

Algorithm 2 Proposed Dynamic Hybrid Beamformer Design

Input: $\{\mathbf{H}_i\}_{i=1}^{N_\mathrm{F}}$, P, b.
Output: $\mathbf{F}_{\mathrm{RF}}^\star, \mathbf{W}_{\mathrm{RF}}^\star, \{\mathbf{F}_{\mathrm{BB},i}^\star, \mathbf{W}_{\mathrm{BB},i}^\star\}_{i=1}^{N_\mathrm{F}}$.
1: Initialize $\mathbf{F}_{\mathrm{RF}}$, $\mathbf{W}_{\mathrm{RF}}$ as (46), and $\{\mathbf{F}_{\mathrm{BB},i}, \mathbf{W}_{\mathrm{BB},i}\}_{i=1}^{N_\mathrm{F}}$ as (47). $\rho_\mathrm{t} = \frac{100}{N_\mathrm{t}}, \rho_\mathrm{r} = \frac{100}{N_\mathrm{r}}$.
2: Set $\mathbf{X}_i = \mathbf{F}_{\mathrm{RF}}\mathbf{F}_{\mathrm{BB},i}$, $\mathbf{Y}_i = \mathbf{W}_{\mathrm{RF}}\mathbf{W}_{\mathrm{BB},i}, \forall i$.
3: **while** no convergence of objective (15a) **do**
4: Update $\{\mathbf{M}_i^\star\}_{i=1}^{N_\mathrm{F}}$ by (17).
5: Update $\{\mathbf{X}_i^\star\}_{i=1}^{N_\mathrm{F}}$ by (21).
6: Update $\{\mathbf{F}_{\mathrm{BB},i}^\star\}_{i=1}^{N_\mathrm{F}}$ by (28).
7: Update $\mathbf{F}_{\mathrm{RF}}^\star$ by Algorithm 1.
8: Update $\{\mathbf{Y}_i^\star\}_{i=1}^{N_\mathrm{F}}$ by (39) and (40).
9: Update $\{\mathbf{W}_{\mathrm{BB},i}^\star\}_{i=1}^{N_\mathrm{F}}$ by (42).
10: Update $\mathbf{W}_{\mathrm{RF}}^\star$ by Algorithm 1.
11: **end while**
12: Normalize $\{\mathbf{F}_{\mathrm{BB},i}^\star\}_{i=1}^{N_\mathrm{F}}$ by (45).
13: Return $\mathbf{F}_{\mathrm{RF}}^\star, \mathbf{W}_{\mathrm{RF}}^\star, \{\mathbf{F}_{\mathrm{BB},i}^\star, \mathbf{W}_{\mathrm{BB},i}^\star\}_{i=1}^{N_\mathrm{F}}$.

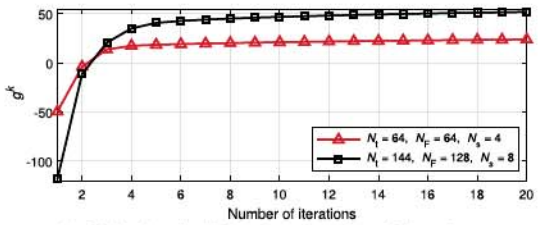

(a) Objective in (19) versus number of iterations.

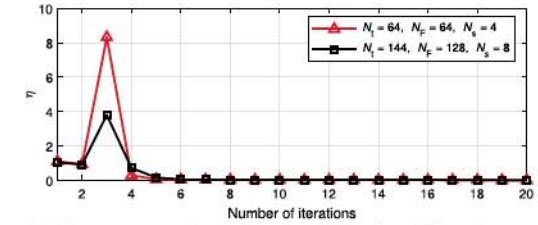

(b) Convergence criterion η versus number of iterations.

Fig. 3. Illustration of convergence for Algorithm 2 ($N_\mathrm{r} = 16$, $N_{\mathrm{RF}}^\mathrm{t} = N_{\mathrm{RF}}^\mathrm{r} = N_\mathrm{s}$, $P = 10$W, $b = 1$).

$$\mathbf{W}_{\mathrm{RF}} = \mathrm{blkdiag}(\mathbf{w}_1, \ldots, \mathbf{w}_{N_{\mathrm{RF}}^\mathrm{r}}), \tag{46c}$$

$$\mathbf{w}_k = \frac{1}{\sqrt{N_\mathrm{r}}} e^{j\mathcal{Q}\{\angle\bar{\mathbf{U}}((k-1)N_\mathrm{r}/N_{\mathrm{RF}}^\mathrm{r}+1:kN_\mathrm{r}/N_{\mathrm{RF}}^\mathrm{r},k)\}}, \quad \forall k, \tag{46d}$$

where the function $\mathcal{Q}(\cdot)$ realizes the quantization operation. Then, we can obtain the effective baseband channel as $\overline{\mathbf{H}}_i \triangleq \mathbf{W}_{\mathrm{RF}}^H \mathbf{H}_i \mathbf{F}_{\mathrm{RF}}, i = 1, \ldots, N_\mathrm{F}$. We again perform a SVD $\overline{\mathbf{H}}_i = \overline{\mathbf{U}}_i \overline{\mathbf{\Sigma}}_i \overline{\mathbf{V}}_i^H$ for each subcarrier. The digital precoder/combiner for each subcarrier is given by

$$\mathbf{F}_{\mathrm{BB},i} = \overline{\mathbf{V}}_i(:, 1:N_\mathrm{s}), \quad \forall i, \tag{47a}$$

$$\mathbf{W}_{\mathrm{BB},i} = \overline{\mathbf{U}}_i(:, 1:N_\mathrm{s}), \quad \forall i. \tag{47b}$$

To satisfy the transmit power constraint, the digital precoders are finally normalized by (45).

IV. Convergence and Complexity Analysis

A. Convergence Analysis

Let g^k be the value of objective in (15) obtained by Algorithm 2 at the k-th iteration. Since the update of each block in Sec. IV-B is optimal with the other variables fixed, the objective in (15) is monotonically nondecreasing after each iteration, i.e.

$$g^k \geq g^{k-1}. \tag{48}$$

Then, we can conclude the proposed algorithm will converge to at least a local optimum since the value of the objective in (15) is bounded above. Fig. 3(a) illustrates g^k as a function of the number of iterations with different settings, which validates the fast convergence of Algorithm 2.

Numerically, we use the relative difference of the objective in (15) at the current and previous iterations as the termination criterion, i.e.

$$\eta \triangleq \frac{|g^k - g^{k-1}|}{|g^{k-1}|} \leq \epsilon, \tag{49}$$

where ϵ is the threshold. Fig. 3(b) shows η versus the number of iterations, which illustrates that the proposed iterative hybrid beamformer design algorithm can easily converge within very few iterations (in this case less than 6). When an arbitrary initialization is used, g^k may become negative in the first two iterations, which results in a large jump of η at the third iteration.

B. Complexity Analysis

Finally, we provide a brief analysis of the complexity of the proposed hybrid beamformer algorithm. As shown in Algorithm 2, in each iteration, step 4 requires a complexity of approximately $\mathcal{O}(N_\mathrm{F} N_\mathrm{s}^3)$ operations, which is mainly caused by the matrix inversion. Step 5 requires $\mathcal{O}(I_1\ N_\mathrm{F} N_\mathrm{t}^3)$ operations, again due to the matrix inversion, where I_1 denotes the number of iterations of the bisection search. Steps 6 and 9 require $\mathcal{O}(N_\mathrm{F} N_\mathrm{t} (N_{\mathrm{RF}}^\mathrm{t})^2)$ and $\mathcal{O}(N_\mathrm{F} N_\mathrm{r} (N_{\mathrm{RF}}^\mathrm{r})^2)$ operations due to the matrix pseudo-inversion, respectively. The order of complexity for steps 7 and 10 is $\mathcal{O}(N_\mathrm{t} N_{\mathrm{RF}}^\mathrm{t} N_\mathrm{s})$ and $\mathcal{O}(N_\mathrm{r} N_{\mathrm{RF}}^\mathrm{r} N_\mathrm{s})$ operations because of the products $\widetilde{\mathbf{F}}_{\mathrm{BB}}(m,:)\widetilde{\mathbf{X}}(n,:)^H$ and $\widetilde{\mathbf{W}}_{\mathrm{BB}}(m,:)\widetilde{\mathbf{Y}}(n,:)^H$, respectively. Finally, step 8 requires $\mathcal{O}(N_\mathrm{F}(N_\mathrm{r} N_\mathrm{s})^3)$ operations due to the inverse of the increased-dimensional matrix involving the Kronecker product. As a result, the overall complexity of the proposed algorithm is given by

$$\mathcal{O}(I_2(N_\mathrm{F} N_\mathrm{s}^3 + I_1\ N_\mathrm{F} N_\mathrm{t}^3 + N_\mathrm{F} N_\mathrm{t} (N_{\mathrm{RF}}^\mathrm{t})^2 + N_\mathrm{F} N_\mathrm{r} (N_{\mathrm{RF}}^\mathrm{r})^2 + N_\mathrm{t} N_{\mathrm{RF}}^\mathrm{t} N_\mathrm{s} + N_\mathrm{r} N_{\mathrm{RF}}^\mathrm{r} N_\mathrm{s} + N_\mathrm{F}(N_\mathrm{r} N_\mathrm{s})^3)) \tag{50a}$$

$$\overset{(a)}{\approx} \mathcal{O}(I_2(I_1\ N_\mathrm{F} N_\mathrm{t}^3 + N_\mathrm{F}(N_\mathrm{r} N_\mathrm{s})^3)) \tag{50b}$$

$$= \mathcal{O}(I_2\ N_\mathrm{F}(I_1 N_\mathrm{t}^3 + N_\mathrm{r}^3 N_\mathrm{s}^3)), \tag{50c}$$

where (a) follows for the typical assumptions $N_\mathrm{s} \leq N_{\mathrm{RF}}^\mathrm{t} \ll N_\mathrm{t}$, $N_\mathrm{s} \leq N_{\mathrm{RF}}^\mathrm{r} \ll N_\mathrm{r}$, and I_2 is the number of iterations for Algorithm 2. The fast convergence behavior demonstrated in Sec. IV-A verifies that the complexity of the proposed algorithm is acceptable even with a large number of transmit/receive antennas and/or subcarriers.

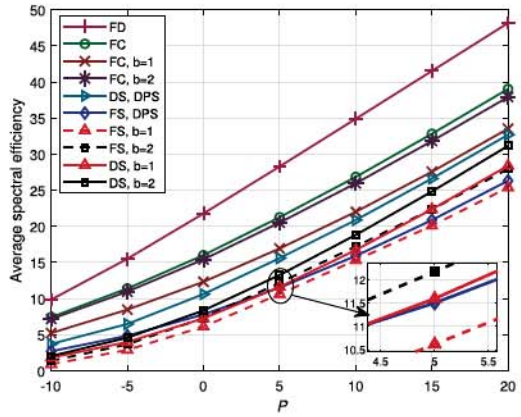

(a) $N_{\mathrm{t}} = 8 \times 8 = 64$, $N_{\mathrm{r}} = 4 \times 4 = 16$, $N_{\mathrm{RF}}^{\mathrm{t}} = N_{\mathrm{RF}}^{\mathrm{r}} = N_s = 4$, $N_{\mathrm{F}} = 64$.

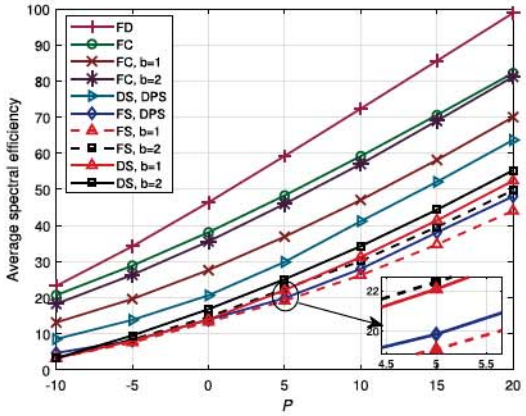

(b) $N_{\mathrm{t}} = 12 \times 12 = 144$, $N_{\mathrm{r}} = 8 \times 8 = 64$, $N_{\mathrm{RF}}^{\mathrm{t}} = N_{\mathrm{RF}}^{\mathrm{r}} = N_s = 8$, $N_{\mathrm{F}} = 128$.

Fig. 4. Average spectral efficiency versus total transmit power P.

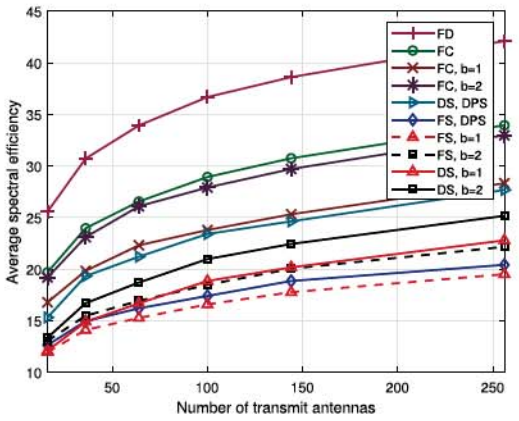

(a) $N_{\mathrm{r}} = 4 \times 4 = 16$.

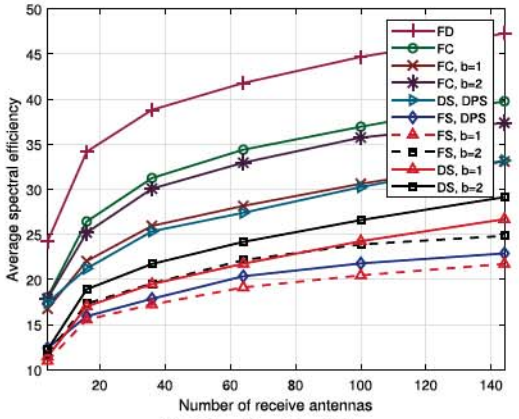

(b) $N_{\mathrm{t}} = 8 \times 8 = 64$.

Fig. 5. Average spectral efficiency versus number of antennas ($N_{\mathrm{F}} = 64$, $N_{\mathrm{RF}}^{\mathrm{t}} = N_{\mathrm{RF}}^{\mathrm{r}} = N_{\mathrm{s}} = 4$, $P = 10$W).

V. Simulation Results

In this section, we present simulation results to demonstrate the performance of the proposed hybrid beamformer design with dynamic subarrays and low-resolution PSs. In the simulation, the channel parameters are set as $L = 10$ paths, carrier frequency $f_{\mathrm{c}} = 60$GHz, bandwidth $B = 1$GHz. Furthermore, azimuth and elevation AoD/AoAs are uniformly distributed over $\left[-\frac{\pi}{2}, \frac{\pi}{2}\right]$ and $\left[-\frac{\pi}{4}, \frac{\pi}{4}\right]$, respectively. The noise powers are set as $\sigma_1^2 = \ldots = \sigma_{N_{\mathrm{F}}}^2 = 1$ for all subcarriers. Finally, the results are averaged over 10^5 channel realizations.

A. Spectral Efficiency

Fig. 4 shows the average spectral efficiency versus the total transmit power P and demonstrates the performance of the proposed hybrid beamformer algorithm for the cases of $b = 1, 2, 3$-bit resolution PSs. For comparison, we also include the following five algorithms: *i*) Fully-digital (FD) beamforming by SVD; *ii*) fully-connected (FC) hybrid beamforming using infinite- and low-resolution PSs [35]; *iii*) *dynamic* subarray hybrid beamforming with *double infinite-resolution* PSs (DS, DPS) [27], which provides a performance upper bound for our algorithm since it uses both more and increased resolution PSs; *iv*) *fixed-subarray* (FS) hybrid beamforming with *double infinite-resolution* PSs (FS, DPS) [27]; *v*) *fixed-subarray* (FS) hybrid beamforming using low-resolution PSs [35] which is a competitor of our proposed algorithm because of its use of a fixed-subarray hybrid beamforming architecture. In [27], the authors treat two PSs with constant amplitudes as equivalent to one PS with variable amplitude and eliminate the amplitude constraint of the analog beamformer. We plot the average spectral efficiency achieved by various algorithms for different parameter settings as shown in Fig. 4(a) and Fig. 4(b), respectively. It is observed that the proposed algorithm always achieves better performance than the fixed-subarray scheme with the same resolutions for all transmit power ranges. When $b = 3$, the proposed algorithm can achieve satisfactory performance close to the dynamic subarray scheme with double infinite-resolution PSs.

In Fig. 5, we show the average spectral efficiency of the proposed algorithm with respect to the number of transmit antennas N_{t} and receive antennas N_{r}. A similar conclusion can be drawn from Fig. 5 that the proposed algorithm can achieve better performance compared with fixed-subarray schemes. We can also expect that the system performance will improve as the number of transmit/receive antennas increases, which can offer more antenna diversity and larger beamforming gain.

In Fig. 6, we show the average spectral efficiency as a function of PS resolution b. As we can predict, the average spectral efficiency will first increase and then gradually tend to saturate with the growth of b. In this case, there is little growth in spectral efficiency beyond about $b \geq 4$, which confirms that

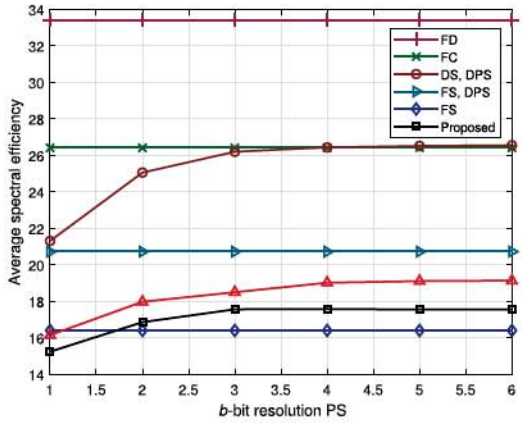

Fig. 6. Average spectral efficiency versus b ($N_{\mathrm{t}} = 8 \times 8 = 64$, $N_{\mathrm{r}} = 4 \times 4 = 16$, $N_{\mathrm{F}} = 64$, $N_{\mathrm{RF}}^{\mathrm{t}} = N_{\mathrm{RF}}^{\mathrm{r}} = N_{\mathrm{s}} = 4$, $P = 10$W).

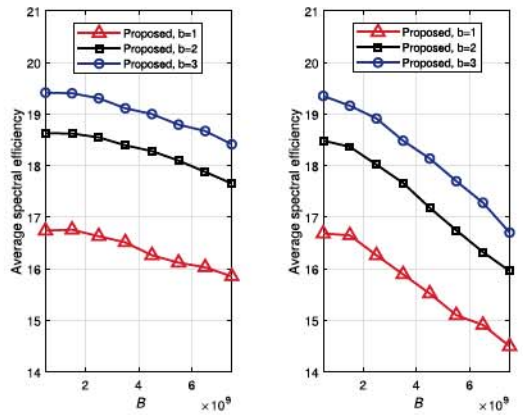

(a) $f_{\mathrm{c}} = 60$GHz. (b) $f_{\mathrm{c}} = 28$GHz.

Fig. 7. Average spectral efficiency versus B ($N_{\mathrm{t}} = 8 \times 8 = 64$, $N_{\mathrm{r}} = 4 \times 4 = 16$, $N_{\mathrm{F}} = 64$, $N_{\mathrm{RF}}^{\mathrm{t}} = N_{\mathrm{RF}}^{\mathrm{r}} = N_{\mathrm{s}} = 4$).

the use of low-resolution PSs is favourable for practical hybrid beamforming schemes. Moreover, with sufficiently large b (e.g. $b \geq 4$), the gap between the proposed algorithm and the "DS, DPS" scheme is due to the fact that the average spectral efficiency of the proposed algorithm is limited by the constant amplitude of each PS whereas for the "DS, DPS" scheme, there is no amplitude constraint.

Fig. 7 illustrates the influence of the bandwidth on the average spectral efficiency. In this figure, we adopt a central carrier frequency $f_{\mathrm{c}} = 60$GHz in Fig. 7(a) and $f_{\mathrm{c}} = 28$GHz in Fig. 7(b). Due to the beam squint effect, there will be increasing variation of the beam steering vector for different subcarriers with a larger bandwidth, which will make it difficult to accurately design the analog precoder/combiner. Thus, the average spectral efficiency will decrease with the growth of the bandwidth. Moreover, with increasing fractional bandwidth (i.e. B/f_{c}), the variation of the beam steering vector will become more severe and thus cause larger performance degradation. Therefore, for wideband mmWave MIMO-OFDM systems, it is necessary to take the beam squint effect into consideration.

B. Energy Efficiency

In order to find the tradeoff between spectral efficiency and energy consumption, we illustrate the energy efficiency of the proposed design as the ratio of the average spectral efficiency and total power consumption, i.e.

$$E \triangleq \frac{\sum_{i=1}^{N_{\mathrm{F}}} R_i}{N_{\mathrm{F}} P_{\mathrm{tot}}}, \tag{51}$$

where P_{tot} is the total power consumption of the transmitter and receiver. The total power consumption for different beamforming architectures is defined in Table II, where P is the transmit power, P_{BB} and P_{RF} are the powers consumed by the baseband processor and a single RF chain, P_{PS} is the energy consumed by a PS, and P_{SW} is the energy consumed by a switch, respectively. In this simulation, we adopt power values for these devices: $P_{\mathrm{RF}} = 300$mW, $P_{\mathrm{BB}} = 200$mW, $P_{\mathrm{PS}}^{\mathrm{inf-res}} = 50$mW (more than 4-bit resolution PSs), $P_{\mathrm{PS}}^{1-\mathrm{bit}} = 10$mW, $P_{\mathrm{PS}}^{2-\mathrm{bit}} = 20$mW, and $P_{\mathrm{SW}} = 5$mW, [24], [50].

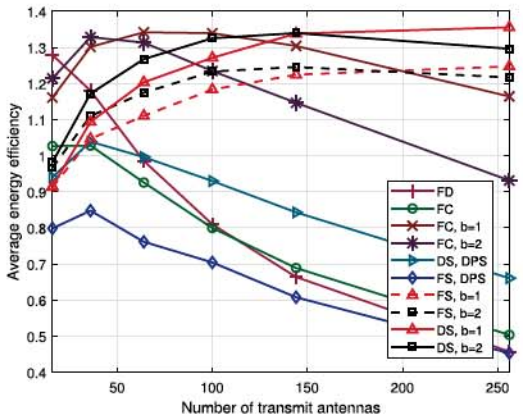

(a) $N_{\mathrm{r}} = 4 \times 4 = 16$.

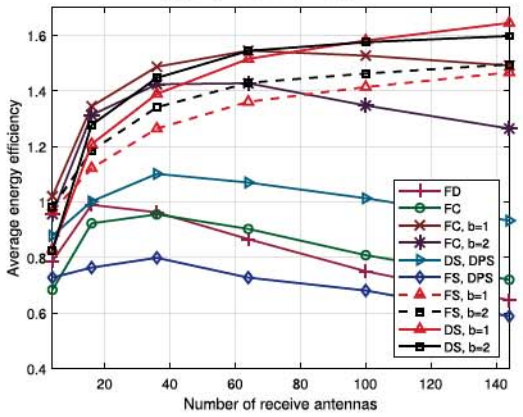

(b) $N_{\mathrm{t}} = 8 \times 8 = 64$.

Fig. 8. Average energy efficiency versus number of antennas ($N_{\mathrm{F}} = 64$, $N_{\mathrm{RF}}^{\mathrm{t}} = N_{\mathrm{RF}}^{\mathrm{r}} = N_{\mathrm{s}} = 4$, $P = 10$W).

In Fig. 8, we plot the energy efficiency as a function of the number of transmit/receive antennas. It is observed in Fig. 8 that the proposed algorithm achieves the best energy performance with large numbers of antennas (e.g. $N_{\mathrm{t}} \geq 144$ in Fig. 8(a) and $N_{\mathrm{r}} > 64$ in Fig. 8(b)). The energy efficiency achieved by the proposed algorithm is slightly lower than the fully-connected scheme when the number of antennas is small, because the power consumed by the PSs for the fully-connected scheme is not significantly greater than that of the combination of additional switches and phase shifters. Therefore, the fully-connected architecture is more suitable for

TABLE II
TOTAL POWER CONSUMPTIONS FOR DIFFERENT ARCHITECTURES IN mmWAVE SYSTEMS

Architecture	Total Power Consumption P_{tot}
Fully-digital (FD)	$P + 2P_{\mathrm{BB}} + N_{\mathrm{t}}P_{\mathrm{RF}} + N_{\mathrm{r}}P_{\mathrm{RF}}$
Fully-connected (FC)	$P + 2P_{\mathrm{BB}} + N_{\mathrm{RF}}^{\mathrm{t}}P_{\mathrm{RF}} + N_{\mathrm{RF}}^{\mathrm{r}}P_{\mathrm{RF}} + N_{\mathrm{t}}N_{\mathrm{RF}}^{\mathrm{t}}P_{\mathrm{PS}} + N_{\mathrm{r}}N_{\mathrm{RF}}^{\mathrm{r}}P_{\mathrm{PS}}$
Dynamic subarray, double PSs (DS, DPS)	$P + 2P_{\mathrm{BB}} + N_{\mathrm{RF}}^{\mathrm{t}}P_{\mathrm{RF}} + N_{\mathrm{RF}}^{\mathrm{r}}P_{\mathrm{RF}} + 2N_{\mathrm{t}}P_{\mathrm{PS}} + 2N_{\mathrm{r}}P_{\mathrm{PS}} + N_{\mathrm{t}}P_{\mathrm{SW}} + N_{\mathrm{r}}P_{\mathrm{SW}}$
Dynamic subarray (DS)	$P + 2P_{\mathrm{BB}} + N_{\mathrm{RF}}^{\mathrm{t}}P_{\mathrm{RF}} + N_{\mathrm{RF}}^{\mathrm{r}}P_{\mathrm{RF}} + N_{\mathrm{t}}P_{\mathrm{PS}} + N_{\mathrm{r}}P_{\mathrm{PS}} + N_{\mathrm{t}}P_{\mathrm{SW}} + N_{\mathrm{r}}P_{\mathrm{SW}}$
Fixed-subarray (FS, DPS)	$P + 2P_{\mathrm{BB}} + N_{\mathrm{RF}}^{\mathrm{t}}P_{\mathrm{RF}} + N_{\mathrm{RF}}^{\mathrm{r}}P_{\mathrm{RF}} + 2N_{\mathrm{t}}P_{\mathrm{PS}} + 2N_{\mathrm{r}}P_{\mathrm{PS}}$
Fixed-subarray (FS)	$P + 2P_{\mathrm{BB}} + N_{\mathrm{RF}}^{\mathrm{t}}P_{\mathrm{RF}} + N_{\mathrm{RF}}^{\mathrm{r}}P_{\mathrm{RF}} + N_{\mathrm{t}}P_{\mathrm{PS}} + N_{\mathrm{r}}P_{\mathrm{PS}}$

small-scale antenna-array cases, while the proposed dynamic subarray architecture is more efficient for cases involving large-scale antenna arrays.

VI. CONCLUSIONS

In this paper, we introduced a novel hardware-efficient hybrid beamforming architecture with dynamic subarrays and low-resolution PSs for wideband mmWave MIMO-OFDM systems. In this dynamic hybrid beamforming scheme, each RF chain is adaptively connected to a disjoint subset of antennas in a large-scale antenna array to increase flexibility and further exploit the multiple-antenna diversity. To optimize the average spectral efficiency, we proposed an iterative hybrid beamformer algorithm with the aid of the relationship between spectral efficiency maximization and MSE minimization. A convergence and complexity analysis of the proposed hybrid beamformer algorithm was also provided. The effectiveness of the proposed hybrid beamformer was validated by extensive simulation results, which illustrated that the proposed algorithm can achieve satisfactory performance and outperform traditional fixed-subarray schemes. For future studies, it is important to take into account the practical imperfections (e.g. insertion losses and phase errors) associated with implementing of dynamic subarrays in wideband mmWave systems. Moreover, it would be interesting to extend the hybrid beamformer architecture with dynamic subarrays and low-resolution PSs to wideband mmWave/Terahertz (THz) multi-user/stream systems.

APPENDIX A
PROOF OF PROPOSITION 1

By checking the first-order optimality conditions of problem (12), i.e.

$$\frac{\partial(\log(|\mathbf{M}_i|) - \mathrm{Tr}\{\mathbf{M}_i\mathsf{E}_i\})}{\partial \mathbf{M}_i} = \mathbf{0}, \quad \forall i, \tag{52a}$$

$$\frac{\partial \mathrm{Tr}\{\mathbf{M}_i\mathsf{E}_i\}}{\partial \mathbf{W}_{\mathrm{BB},i}} = \mathbf{0}, \quad \forall i, \tag{52b}$$

we can obtain the optimal $\mathbf{M}_i$ and $\mathbf{W}_{\mathrm{BB},i}$ as

$$\mathbf{M}_i^{\star} = \mathsf{E}_i^{-1}, \forall i, \tag{53}$$

$$\mathbf{W}_{\mathrm{BB},i}^{\star} = (\mathbf{W}_{\mathrm{RF}}^H\mathbf{A}_i\mathbf{W}_{\mathrm{RF}})^{-1}\mathbf{W}_{\mathrm{RF}}^H\mathbf{H}_i\mathbf{F}_{\mathrm{RF}}\mathbf{F}_{\mathrm{BB},i}, \quad \forall i, \tag{54}$$

where

$$\mathbf{A}_i \triangleq \mathbf{H}_i\mathbf{F}_{\mathrm{RF}}\mathbf{F}_{\mathrm{BB},i}\mathbf{F}_{\mathrm{BB},i}^H\mathbf{F}_{\mathrm{RF}}^H\mathbf{H}_i^H + \sigma_i^2\mathbf{I}, \quad \forall i. \tag{55}$$

From equation (54) we can see that the optimal digital combiner for problem (12) is the well-known MMSE receiver. After substituting (54) into (53), we have [51]

$$\mathbf{M}_i^{\star} = [\mathbf{I} - \mathbf{F}_{\mathrm{BB},i}^H\mathbf{F}_{\mathrm{RF}}^H\mathbf{H}_i^H\mathbf{W}_{\mathrm{RF}}(\mathbf{W}_{\mathrm{RF}}^H\mathbf{A}_i\mathbf{W}_{\mathrm{RF}})^{-1} \times \mathbf{W}_{\mathrm{RF}}^H\mathbf{H}_i\mathbf{F}_{\mathrm{RF}}\mathbf{F}_{\mathrm{BB},i}]^{-1} \tag{56a}$$

$$= \mathbf{I} + \mathbf{F}_{\mathrm{BB},i}^H\mathbf{F}_{\mathrm{RF}}^H\mathbf{H}_i^H\mathbf{W}_{\mathrm{RF}}\widetilde{\Upsilon}_i^{-1}\mathbf{W}_{\mathrm{RF}}^H\mathbf{H}_i\mathbf{F}_{\mathrm{RF}}\mathbf{F}_{\mathrm{BB},i}, \quad \forall i, \tag{56b}$$

where we define $\tilde{\Upsilon}_i \triangleq \sigma_i^2\mathbf{W}_{\mathrm{RF}}^H\mathbf{W}_{\mathrm{RF}}$. Then substituting (54) and (56b) into the objective in (12), we can obtain [51]

$$\log(|\mathbf{M}_i^{\star}|) - \mathrm{Tr}\{\mathbf{M}_i^{\star}\mathsf{E}_i\} + N_{\mathrm{s}} = \log(|\mathbf{I} + \mathbf{F}_{\mathrm{BB},i}^H\mathbf{F}_{\mathrm{RF}}^H\mathbf{H}_i^H\mathbf{W}_{\mathrm{RF}}\widetilde{\Upsilon}_i^{-1}\mathbf{W}_{\mathrm{RF}}^H\mathbf{H}_i\mathbf{F}_{\mathrm{RF}}\mathbf{F}_{\mathrm{BB},i}|) \tag{57a}$$

$$= \log(|\mathbf{I} + \widetilde{\Upsilon}_i^{-1}\mathbf{W}_{\mathrm{RF}}^H\mathbf{H}_i\mathbf{F}_{\mathrm{RF}}\mathbf{F}_{\mathrm{BB},i}\mathbf{F}_{\mathrm{BB},i}^H\mathbf{F}_{\mathrm{RF}}^H\mathbf{H}_i^H\mathbf{W}_{\mathrm{RF}}|), \quad \forall i, \tag{57b}$$

which is essentially the spectral efficiency of the i-th subcarrier without considering the digital combiner. This result implies that the globally optimal solution of the weighted MSE minimization problem in (12) is identical to the solution obtained by maximizing the spectral efficiency in (57).

We recall the original spectral efficiency maximization problem (10), where the digital combiner $\mathbf{W}_{\mathrm{BB},i}, i = 1, \ldots, N_{\mathrm{F}}$, does not have any constraint. It is well-known that the optimal MMSE digital combiner can achieve maximum spectral efficiency [14], [46]. Thus, optimal solutions of (12) are also identical to (10) and the proof is completed. ■

APPENDIX B
PROOF OF PROPOSITION 2

Recall that $\mathcal{D}_m^{\mathrm{t}}, m = 1, \ldots, N_{\mathrm{RF}}^{\mathrm{t}}$, are the dynamic subarray sets containing the indices of the transmit antennas connected to the m-th RF chain. Since there is no overlap among the dynamic subarrays and each transmit antenna is connected to one RF chain, we have: *i)* $\mathcal{D}_p^{\mathrm{t}} \cap \mathcal{D}_q^{\mathrm{t}} = \varnothing, p, q = 1, \ldots, N_{\mathrm{RF}}^{\mathrm{t}}, p \neq q$; *ii)* $\cup_{m=1}^{N_{\mathrm{RF}}^{\mathrm{t}}}\mathcal{D}_m^{\mathrm{t}} = \mathcal{N}_{\mathrm{t}} \triangleq \{1, \ldots, N_{\mathrm{t}}\}$. With the above constraints, it can be shown that

$$\min_{\mathbf{F}_{\mathrm{RF}}} \sum_{i=1}^{N_{\mathrm{F}}} \|\mathbf{X}_i - \mathbf{F}_{\mathrm{RF}}\mathbf{F}_{\mathrm{BB},i}\|_F^2 \tag{58a}$$

$$= \min_{\mathbf{F}_{\mathrm{RF}}} \|\widetilde{\mathbf{X}} - \mathbf{F}_{\mathrm{RF}}\widetilde{\mathbf{F}}_{\mathrm{BB}}\|_F^2 \tag{58b}$$

$$\overset{(a)}{=} \min_{\mathbf{F}_{\mathrm{RF}}} \sum_{m=1}^{N_{\mathrm{RF}}^{\mathrm{t}}} \sum_{n\in\mathcal{D}_m^{\mathrm{t}}} \|\widetilde{\mathbf{X}}(n,:) - \mathbf{F}_{\mathrm{RF}}(n,m)\widetilde{\mathbf{F}}_{\mathrm{BB}}(m,:)\|_2^2 \tag{58c}$$

$$= \min_{\mathbf{F}_{\mathrm{RF}}} \sum_{m=1}^{N_{\mathrm{RF}}^{\mathrm{t}}} \sum_{n\in\mathcal{D}_m^{\mathrm{t}}} (\|\widetilde{\mathbf{X}}(n,:)\|^2 - 2\Re\{\mathbf{F}_{\mathrm{RF}}(n,m)\widetilde{\mathbf{F}}_{\mathrm{BB}}(m,:) \times \widetilde{\mathbf{X}}(n,:)^H\} + |\mathbf{F}_{\mathrm{RF}}(n,m)|^2\|\widetilde{\mathbf{F}}_{\mathrm{BB}}(m,:)\|_2^2) \tag{58d}$$

$$\overset{(b)}{=} \max_{\mathbf{F}_{\mathrm{RF}}} \sum_{m=1}^{N_{\mathrm{RF}}^{\mathrm{t}}} \sum_{n\in\mathcal{D}_m^{\mathrm{t}}} \Re\{\mathbf{F}_{\mathrm{RF}}(n,m)\widetilde{\mathbf{F}}_{\mathrm{BB}}(m,:)\widetilde{\mathbf{X}}(n,:)^H\}, \tag{58e}$$

where (a) holds since there is only one nonzero element in each row (corresponding to each transmit antenna) of the analog beamformer; (b) holds since each nonzero element has constant magnitude $\frac{1}{\sqrt{N_{\mathrm{t}}}}$, i.e. $|\mathbf{F}_{\mathrm{RF}}(n,m)|^2 = \frac{1}{N_{\mathrm{t}}}$.

By defining $\varpi_{m,n}^{\mathrm{t}} \triangleq \widetilde{\mathbf{F}}_{\mathrm{BB}}(m,:)\widetilde{\mathbf{X}}(n,:)^H = |\varpi_{m,n}^{\mathrm{t}}|e^{j\zeta_{m,n}^{\mathrm{t}}}$, $m = 1,\ldots,N_{\mathrm{RF}}^{\mathrm{t}}, n \in \mathcal{D}_m^{\mathrm{t}}$ and $\mathbf{F}_{\mathrm{RF}}(n,m) \triangleq \frac{1}{\sqrt{N_{\mathrm{t}}}}e^{j\xi_{m,n}^{\mathrm{t}}}$ with discrete values $\xi_{m,n}^{\mathrm{t}} \in \mathcal{B} \triangleq \{\frac{2\pi i}{2^b} | i = 0,1,\ldots,2^b-1\}$, the objective (58e) can be rewritten as

$$\max_{\substack{\{\xi_{m,n}^{\mathrm{t}},\forall m,n\}\\ \{\mathcal{D}_m^{\mathrm{t}}\}_{m=1}^{N_{\mathrm{RF}}^{\mathrm{t}}}}} \sum_{m=1}^{N_{\mathrm{RF}}^{\mathrm{t}}} \sum_{n\in\mathcal{D}_m^{\mathrm{t}}} |\varpi_{m,n}^{\mathrm{t}}| \cos(\zeta_{m,n}^{\mathrm{t}} + \xi_{m,n}^{\mathrm{t}}). \tag{59}$$

Combining the objective (59) and the two constraints corresponding to the dynamic subarray sets and discrete values of the analog beamformer, the equivalence of problem (29) and (31) is finally established. ■

REFERENCES

[1] Z. Pi and F. Khan, "An introduction to millimeter-wave mobile broadband systems," *IEEE Commun. Mag.*, vol. 49, no. 6, pp. 101–107, Jun. 2011.

[2] A. L. Swindlehurst, E. Ayanoglu, P. Heydari, and F. Capolino, "Millimeter-wave massive MIMO: The next wireless resolution?" *IEEE Commun. Mag.*, vol. 52, no. 9, pp. 56–62, Sep. 2014.

[3] R. W. Heath, Jr., N. Gonzalez-Prelcic, S. Rangan, W. Roh, and A. M. Sayeed, "An overview of signal processing techniques for millimeter wave MIMO systems," *IEEE J. Sel. Topics Signal Process.*, vol. 10, no. 3, pp. 436–453, Apr. 2016.

[4] A. S. Y. Poon and M. Taghivand, "Supporting and enabling circuits for antenna arrays in wireless communications," *Proc. IEEE*, vol. 100, no. 7, pp. 2207–2218, Jul. 2012.

[5] E. Björnson, E. G. Larsson, and T. L. Marzetta, "Massive MIMO: Ten myths and one critical question," *IEEE Commun. Mag.*, vol. 54, no. 2, pp. 114–123, Feb. 2016.

[6] A. Alkhateeb, J. Mo, N. González-Prelcic, and R. W. Heath, Jr., "MIMO precoding and combining for millimeter-wave systems," *IEEE Commun. Mag.*, vol. 52, no. 12, pp. 122–131, Dec. 2014.

[7] E. Bjornson, L. Van der Perre, S. Buzzi, and E. G. Larsson, "Massive MIMO in sub-6 GHz and mmWave: Physical, practical, and use-case differences," *IEEE Wireless Commun.*, vol. 26, no. 2, pp. 100–108, Apr. 2019.

[8] J. Zhang, L. Dai, X. Li, Y. Liu, and L. Hanzo, "On low-resolution ADCs in practical 5G millimeter-wave massive MIMO systems," *IEEE Commun. Mag.*, vol. 56, no. 7, pp. 205–211, Jul. 2018.

[9] X. Yu, J.-C. Shen, J. Zhang, and K. B. Letaief, "Alternating minimization algorithms for hybrid precoding in millimeter wave MIMO systems," *IEEE J. Sel. Topics Signal Process.*, vol. 10, no. 3, pp. 485–500, Apr. 2016.

[10] C.-E. Chen, "An iterative hybrid transceiver design algorithm for millimeter wave MIMO systems," *IEEE Wireless Commun. Lett.*, vol. 4, no. 3, pp. 285–288, Jun. 2015.

[11] O. E. Ayach, S. Rajagopal, S. Abu-Surra, Z. Pi, and R. W. Heath, Jr., "Spatially sparse precoding in millimeter wave MIMO systems," *IEEE Trans. Wireless Commun.*, vol. 13, no. 3, pp. 1499–1513, Mar. 2014.

[12] J. Zhang, Y. Huang, Q. Shi, J. Wang, and L. Yang, "Codebook design for beam alignment in millimeter wave communication systems," *IEEE Trans. Commun.*, vol. 65, no. 11, pp. 4980–4995, Nov. 2017.

[13] S. He, J. Wang, Y. Huang, B. Ottersten, and W. Hong, "Codebook-based hybrid precoding for millimeter wave multiuser systems," *IEEE Trans. Signal Process.*, vol. 65, no. 20, pp. 5289–5304, Oct. 2017.

[14] Q. Shi and M. Hong, "Spectral efficiency optimization for millimeter wave multiuser MIMO systems," *IEEE J. Sel. Topics Signal Process.*, vol. 12, no. 3, pp. 455–468, Jun. 2018.

[15] J. Du, W. Xu, C. Zhao, and L. Vandendorpe, "Weighted spectral efficiency optimization for hybrid beamforming in multiuser massive MIMO-OFDM systems," *IEEE Trans. Veh. Technol.*, vol. 68, no. 10, pp. 9698–9712, Oct. 2019.

[16] T. Lin, Y. Zhu, J. Zhang, and K. B. Letaief, "Hybrid beamforming for millimeter wave systems using the MMSE criterion," *IEEE Trans. Commun.*, vol. 67, no. 5, pp. 3698–3703, May 2019.

[17] O. E. Ayach, R. W. Heath, Jr., S. Rajagopal, and Z. Pi, "Multimode precoding in millimeter wave MIMO transmitters with multiple antenna sub-arrays," in *Proc. IEEE Global Commun. Conf. (GLOBECOM)*, Atlanta, GA, USA, Dec. 2013, pp. 3476–3480.

[18] X. Gao, L. Dai, S. Han, C.-L. I, and R. W. Heath, Jr., "Energy-efficient hybrid analog and digital precoding for mmWave MIMO systems with large antenna arrays," *IEEE J. Sel. Areas Commun.*, vol. 34, no. 4, pp. 998–1009, Apr. 2016.

[19] S. He, C. Qi, Y. Wu, and Y. Huang, "Energy-efficient transceiver design for hybrid sub-array architecture MIMO systems," *IEEE Access*, vol. 4, pp. 9895–9905, 2016.

[20] M. Li, Z. Wang, H. Li, Q. Liu, and L. Zhou, "A hardware-efficient hybrid beamforming solution for mmWave MIMO systems," *IEEE Wireless Commun.*, vol. 26, no. 1, pp. 137–143, Feb. 2019.

[21] J.-C. Chen, "Hybrid beamforming with discrete phase shifters for millimeter-wave massive MIMO systems," *IEEE Trans. Veh. Technol.*, vol. 66, no. 8, pp. 7604–7608, Aug. 2017.

[22] Z. Wang, M. Li, Q. Liu, and A. L. Swindlehurst, "Hybrid precoder and combiner design with low-resolution phase shifters in mmWave MIMO systems," *IEEE J. Sel. Topics Signal Process.*, vol. 12, no. 2, pp. 256–269, May 2018.

[23] Z. Lu, Y. Zhang, and J. Zhang, "Quantized hybrid precoding design for millimeter-wave large-scale MIMO systems," *China Commun.*, vol. 16, no. 4, pp. 130–138, Apr. 2019.

[24] X. Gao, L. Dai, Y. Sun, S. Han, and I. Chih-Lin, "Machine learning inspired energy-efficient hybrid precoding for mmWave massive MIMO systems," in *Proc. IEEE Int. Conf. Commun. (ICC)*, Paris, France, May 2017.

[25] Z. Wang, M. Li, H. Li, and Q. Liu, "Hybrid beamforming with one-bit quantized phase shifters in mmWave MIMO systems," in *Proc. IEEE Int. Conf. Commun. (ICC)*, Kansas City, MO, USA, May 2018, pp. 1–6.

[26] S. Park, A. Alkhateeb, and R. W. Heath, Jr., "Dynamic subarrays for hybrid precoding wideband mmWave MIMO systems," *IEEE Trans. Wireless Commun.*, vol. 16, no. 5, pp. 2907–2920, May 2017.

[27] X. Yu, J. Zhang, and K. B. Letaief, "Partially-connected hybrid precoding in mm-wave systems with dynamic phase shifter networks," in *Proc. IEEE 18th Int. Workshop Signal Process. Adv. Wireless Commun. (SPAWC)*, Sapporo, Japan, Jul. 2017, pp. 1–5.

[28] Y. Sun, Z. Gao, H. Wang, and D. Wu, "Machine learning based hybrid precoding for mmWave MIMO-OFDM with dynamic subarray," in *Proc. IEEE Globecom Workshops (GC Wkshps)*, Abu Dhabi, United Arab Emirates, Dec. 2018, pp. 1–6.

[29] L. Zhang, L. Gui, K. Ying, and Q. Qin, "Clustering based hybrid precoding design for multiuser massive MIMO systems," *IEEE Trans. Veh. Technol.*, vol. 68, no. 12, pp. 12164–12178, Dec. 2019.

[30] J. Jin, C. Xiao, W. Chen, and Y. Wu, "Hybrid precoding in mmWave MIMO broadcast channels with dynamic subarrays and finite-alphabet inputs," in *Proc. IEEE Int. Conf. Commun. (ICC)*, Kansas City, MO, USA, May 2018, pp. 1–6.

[31] H. Li, Z. Wang, M. Li, and W. Kellerer, "Efficient analog beamforming with dynamic subarrays for mmWave MU-MISO systems," in *Proc. IEEE 89th Veh. Technol. Conf. (VTC-Spring)*, Kuala Lumpur, Malaysia, Apr. 2019, pp. 1–5.

[32] H. Li, Q. Liu, Z. Wang, and M. Li, "Transmit antenna selection and analog beamforming with low-resolution phase shifters in mmWave MISO systems," *IEEE Commun. Lett.*, vol. 22, no. 9, pp. 1878–1881, Sep. 2018.

[33] H. Li, Q. Liu, Z. Wang, and M. Li, "Joint antenna selection and analog precoder design with low-resolution phase shifters," *IEEE Trans. Veh. Technol.*, vol. 68, no. 1, pp. 967–971, Jan. 2019.
[34] H. Li, M. Li, and Q. Liu, "Hybrid beamforming with dynamic subarrays and low-resolution PSs for mmWave MU-MISO systems," *IEEE Trans. Commun.*, vol. 68, no. 1, pp. 602–614, Jan. 2020.
[35] F. Sohrabi and W. Yu, "Hybrid analog and digital beamforming for mmWave OFDM large-scale antenna arrays," *IEEE J. Sel. Areas Commun.*, vol. 35, no. 7, pp. 1432–1443, Jul. 2017.
[36] A. Alkhateeb and R. W. Heath, Jr., "Frequency selective hybrid precoding for limited feedback millimeter wave systems," *IEEE Trans. Commun.*, vol. 64, no. 5, pp. 1801–1818, May 2016.
[37] Y. Kwon, J. Chung, and Y. Sung, "Hybrid beamformer design for mmWave wideband multiuser MIMO-OFDM systems: (Invited paper)," in *Proc. IEEE 18th Int. Workshop Signal Process. Adv. Wireless Commun. (SPAWC)*, Sapporo, Japan, Jul. 2017, pp. 1–5.
[38] B. Wang, F. Gao, S. Jin, H. Lin, and G. Y. Li, "Spatial- and frequency-wideband effects in millimeter-wave massive MIMO systems," *IEEE Trans. Signal Process.*, vol. 66, no. 13, pp. 3393–3406, Jul. 2018.
[39] M. Wang, F. Gao, S. Jin, and H. Lin, "An overview of enhanced massive MIMO with array signal processing techniques," *IEEE J. Sel. Topics Signal Process.*, vol. 13, no. 5, pp. 886–901, Sep. 2019.
[40] M. Cai *et al.*, "Effect of wideband beam squint on codebook design in phased-array wireless systems," in *Proc. IEEE Global Commun. Conf. (GLOBECOM)*, Washington, DC, USA, Dec. 2016, pp. 1–6.
[41] B. Liu, W. Tan, H. Hu, and H. Zhu, "Hybrid beamforming for mmWave MIMO-OFDM system with beam squint," in *Proc. IEEE 29th Annu. Int. Symp. Pers., Indoor Mobile Radio Commun. (PIMRC)*, Bologna, Italy, Sep. 2018, pp. 1422–1426.
[42] J. P. Gonzalez-Coma, W. Utschick, and L. Castedo, "Hybrid LISA for wideband multiuser millimeter-wave communication systems under beam squint," *IEEE Trans. Wireless Commun.*, vol. 18, no. 2, pp. 1277–1288, Feb. 2019.
[43] D. Liu, U. Pfeiffer, B. Gaucher, and J. Grzyb, *Advanced Millimeter-wave Technologies: Antennas, Packaging and Circuits*. New York, NY, USA: Wiley, 2009.
[44] P. Smulders, "Statistical characterization of 60-GHz indoor radio channels," *IEEE Trans. Antennas Propag.*, vol. 57, no. 10, pp. 2820–2829, Oct. 2009.
[45] T. S. Rappaport, G. R. MacCartney, M. K. Samimi, and S. Sun, "Wideband millimeter-wave propagation measurements and channel models for future wireless communication system design," *IEEE Trans. Commun.*, vol. 63, no. 9, pp. 3029–3056, Sep. 2015.
[46] Q. Shi, M. Razaviyayn, Z.-Q. Luo, and C. He, "An iteratively weighted MMSE approach to distributed sum-utility maximization for a MIMO interfering broadcast channel," *IEEE Trans. Signal Process.*, vol. 59, no. 9, pp. 4331–4340, Sep. 2011.
[47] D. Bertsekas, *Nonlinear Programming*, 2nd ed. Belmont, MA, USA: Athena Scientific, 1999.
[48] Q. Shi, M. Hong, X. Fu, and T.-H. Chang, "Penalty dual decomposition method for nonsmooth nonconvex optimization," 2017, *arXiv:1712.04767*. [Online]. Available: http://arxiv.org/abs/1712.04767
[49] J. D. Gardiner, A. J. Laub, J. J. Amato, and C. B. Moler, "Solution of the Sylvester matrix equation $AXB^T + CXD^T = E$," *ACM Trans. Math. Softw.*, vol. 18, no. 2, pp. 223–231, Jun. 1992.
[50] R. Mendez-Rial, C. Rusu, N. Gonzalez-Prelcic, A. Alkhateeb, and R. W. Heath, Jr., "Hybrid MIMO architectures for millimeter wave communications: Phase shifters or switches?" *IEEE Access*, vol. 4, pp. 247–267, 2016.
[51] G. H. Golub and C. F. Van Loan, *Matrix Computations*. Baltimore, MD, USA: The Johns Hopkins Univ. Press, 2012.

Hongyu Li (Graduate Student Member, IEEE) received the B.S. degree in electronics information engineering from the Dalian University of Technology, Dalian, China, in 2018, where she is currently pursuing the M.S. degree with the School of Information and Communication Engineering.

Her current research interests are focused on signal processing, mmWave communications, and massive MIMO systems.

Ming Li (Senior Member, IEEE) received the M.S. and Ph.D. degrees in electrical engineering from the State University of New York at Buffalo (SUNY-Buffalo), Buffalo, in 2005 and 2010, respectively.

From January 2011 to August 2013, he was a Post-Doctoral Research Associate with the Signals, Communications, and Networking Research Group, Department of Electrical Engineering, SUNY-Buffalo. From August 2013 to June 2014, he was with Qualcomm Technologies Inc. as a Senior Engineer. Since June 2014, he has been with the School of Information and Communication Engineering, Dalian University of Technology, Dalian, China, where he is currently an Associate Professor. His current research interests are in the general areas of communication theory and signal processing with applications to mmWave communications, secure wireless communications, cognitive radios and networks, data hiding and steganography.

Qian Liu (Member, IEEE) received the B.S. and M.S. degrees from the Dalian University of Technology, Dalian, China, in 2006 and 2009, respectively, and the Ph.D. degree from the State University of New York at Buffalo (SUNY-Buffalo), Buffalo, NY, USA, in 2013.

She was a Post-Doctoral Fellow with Ubiquitous Multimedia Laboratory, SUNY-Buffalo, from 2013 to 2015. She received the Alexander von Humboldt Fellowship in 2015, and was a Post-Doctoral Fellow with the Chair of Media Technology and the Chair of Communication Networks, Technical University of Munich, from 2016 to 2017. She is currently an Associate Professor with the School of Computer Science and Technology, Dalian University of Technology, China. Her current research interests include multimedia transmission over MIMO systems, IEEE 802.11 wireless networks and LTE networks, device-to-device communication, energy-aware multimedia delivery, and the tactile Internet. She received the Best Paper Runner-up Award at the 2012 IEEE International Conference on Multimedia and Expo and was in the finalist for the Best Student Paper Award at the 2011 IEEE International Symposium on Circuits and Systems.

A. Lee Swindlehurst (Fellow, IEEE) received the B.S. and M.S. degrees in electrical engineering from Brigham Young University (BYU) in 1985 and 1986, respectively, and the Ph.D. degree in electrical engineering from Stanford University in 1991. He was with the Department of Electrical and Computer Engineering, BYU, from 1990 to 2007, where he served as a Department Chair from 2003 to2006. From 1996 to 1997, he held a joint appointment as a Visiting Scholar at Uppsala University and the Royal Institute of Technology, Sweden. From 2006 to 2007, he was on leave working as a Vice President of Research for ArrayComm LLC, San Jose, California. Since 2007, he has been a Professor with Electrical Engineering and Computer Science Department, University of California Irvine, where he served as an Associate Dean for Research and Graduate Studies at the Samueli School of Engineering from 2013 to 2016. From 2014 to 2017, he was also a Hans Fischer Senior Fellow with the Institute for Advanced Studies, Technical University of Munich. In 2016, he was elected as a Foreign Member of the Royal Swedish Academy of Engineering Sciences (IVA). His research focuses on array signal processing for radar, wireless communications, and biomedical applications, and he has over 300 publications in these areas. He received the 2000 IEEE W. R. G. Baker Prize Paper Award, the 2006 IEEE Communications Society Stephen O. Rice Prize in the field of communication theory, the 2006 and 2010 IEEE Signal Processing Societys Best Paper Awards, and the 2017 IEEE Signal Processing Society Donald G. Fink Overview Paper Award. He was the inaugural Editor-in-Chief of the IEEE JOURNAL OF SELECTED TOPICS IN SIGNAL PROCESSING.